WELDING OF DISSIMILAR METALS

Submitted in Partial fulfilment of the requirement

For the award of the degree of

MASTER OF TECHNOLOGY

IN

PRODUCTION ENGINEERING

Submitted by:

Adhirath Mandal (2K12/PRD/02)

Under the Supervision and Guidance of

Prof. Reeta Wattal

DEPARTMENT OF MECHANICAL, PRODUCTION & INDUSTRIAL AND AUTOMOBILE ENGINEERING

DELHI TECHNOLOGICAL UNIVERSITY

BAWANA ROAD, DELHI

2015

DEDICATED TO MY

GRANDPARENTS

STUDENTS DECLARATION

This is to certify that thesis entitled, "***Welding of Dissimilar Matals* "** submitted by **Mr. Adhirath Mandal** (Roll No.: **2K12/PRD/02**) is an authentic record of own work carried out by me. I also certify that there is no plagiarism material in this report and has not been submitted to any other Institute/University for the award of any degree or diploma.

Dated

Adhirath Mandal
(2K12/PRD/25)
M.Tech (Production Engineering)
Delhi Technological University

CERTIFICATE

This is to certify that thesis entitled, "**Welding of Dissimilar Metals**" submitted by Mr. Adhirath Mandal in partial fulfillment of the requirements for the award of Master Of Technology in Mechanical Engineering with "Production Engineering" Specialization during session 2012-2014 in the Department of Mechanical engineering, Delhi Technological University, Delhi.

This work is carried out by him under my supervision and guidance. To the best of my knowledge, the matter embodied in this thesis has not been submitted to any other University/Institute for award of any Degree or Diploma.

Dr (Mrs) Reeta Wattal
Professor,
Department of Mechanical Engineering,
Delhi Technological University,
Delhi

ACKNOWLEDGEMENT

I express my deep sense of gratitude and indebtedness to my thesis supervisor **Dr. Reeta Wattal, Professor, Department of Mechanical Engineering, DTU** for providing precious guidance, inspiring discussions and constant supervision throughout the course of this work. Her timely help, constructive criticism, and conscientious efforts made it possible to present the work contained in this thesis.

I am grateful to **Prof. R.S Mishra**, Head, Mechanical Engineering Department, **Shri Vijay Gautam**, Assistant Professor, Delhi Technological University for providing facilities to carry out the investigations.

I wish to express my warm and sincere thanks to Ms. Deepanjali Nimker, Mr. Ramakant Rana, Mr Pushp Kr. Baghel & Mr Ujjwal Chauhan who helped me in every phase of this project to get the constructive ideas which had a remarkable influence on my entire thesis.

I cannot close these prefatory remarks without expressing my deep sense of gratitude and reverence to my dear parents for their blessings and Endeavour to keep my moral high throughout the period of my work.

Above all, I express my indebtedness to the "ALMIGHTY" for all his blessings and kindness. I feel pleased and privileged to fulfill my family's ambition and I am greatly indebted to them for bearing the inconvenience during my M Tech. course.

Adhirath Mandal
Roll NO: 2K12/PRD/02
M.Tech (Production Engineering)
Delhi Technological University

ABSTRACT

In heat exchangers, tubing is required for the passage of the working fluid throughout the heat exchanger circuit. The requirement of the tubing inside the heat exchanger is of high heat transfer rate, thermal conductivity and ductility. For this purpose, Copper tubes are being used in the industry because they serve the above requirements optimally. But due to economic constraints their usage throughout the heat exchanger circuit is not profitable. For the rest of the tubing outside the heat exchanger, Stainless Steel tubes are used because of economic considerations and good corrosion resistance. Therefore replacement of copper components by stainless steel can be an attractive way to overcome the difficulty. There are different methods to weld copper with stainless steel and these are arc welding, diffusion bonding, laser beam welding and electron beam welding. Literature survey indicated that limited work has been reported on welding of dissimilar metal (copper with stainless steel) by gas tungsten arc welding method.

GTAW offers many advantages such as it is relatively inexpensive, it offers an inert gas atmosphere at the weld using argon gas, which protects the weld pool from reacting with oxygen. This results in a more successful weld, the welding process is compatible with most product designs and so it offer flexibility. The equipment is relatively easy to use. The above reasons led to attempt weld copper with stainless steel using the GTAW process in this project.

Keyword: GTAW, Tensile strength, Micro structure, Micro hardness, full factorial design

TABLE OF CONTENTS

LIST OF FIGURES

LIST OF TABLES

CHAPTER 1

INTRODUCTION

1.1. COPPER: AN INTRODUCTION

Copper is a chemical element with the symbol Cu and atomic number 29. In the periodic table of elements copper is in the same group as gold and silver. It shares many of the same characteristics, with gold and silver to the point of being defined a "semi" noble metal if not a true noble metal. It has a very high thermal and electrical conductivity. It is a ductile semi-precious metal. Pure copper is soft and malleable. The exposed surface has a reddish-orange tarnish color.

1.2. APPLICATION OF COPPER

The physical-chemical properties of copper are the key factors in the success of this material and its extensive and diversified use. Its parameters in terms of reliability, longevity, safety, workability, protection of human health, and environmental sustainability are a guarantee for the industries and end users of this products. Copper's extremely high electrical conductivity is absolutely key for its use in the electric and electronics industries. Copper's acquisition of excellent thermal conductivity, heat, pressure resistance, antibacterial properties and reliability has been the reason for making it as reference material for heating systems, drinking water, air conditioning / refrigeration and gas tubing. Coper’s aesthetic characteristics durability, corrosion resistance and mechanical behavior are critical factors for its architectural applications, as well as for mechanical components, transport vehicles, consumer goods, minting, and in the marine industry. Copper is one of the most versatile engineering material. The combination of copper properties such as strength, conductivity, corrosion resistance, machinability and ductility make copper suitable for wide range of applications.

1.3. STAINLESS STEEL: AN INTRODUCTION

Stainless steel is essentially a low carbon steel which contains 10% chromium or more by weight. Addition of chromium that gives the steel its unique stainless and corrosion resisting properties. The corrosion resistant and other useful properties of the steel are enhanced by increasing the chromium content and by the addition of other elements such as molybdenum, nickel and nitrogen.

There are more than 60 grades of stainless steel. However, the entire group can be divided into five classes. Each is identified by the alloying elements which affect their microstructure and has been named separately.

1.4. TYPES OF STAINLESS STEEL

There are different types of stainless steels: when nickel is added, for instance, the austenite structure of iron is stabilized. This crystal structure makes such steels non-magnetic and less brittle at low temperatures. Carbon is added for higher hardness and strength. Significant quantities of manganese have been used in many stainless steel compositions. Manganese preserves the austenitic structure of the steel as does nickel, but at a lower cost.

Stainless steels are also classified by their crystalline structure:

I. **Austenitic stainless steels:** It comprise over 70% of total stainless steel production. They contain a maximum of 0.15% carbon, a minimum of 16% chromium and sufficient nickel and/or manganese to retain an austenitic structure at all temperatures from the cryogenic region to the melting point of the alloy.

II. **Ferritic stainless steels:** They are highly corrosion resistant, but far less durable than austenitic grades. It cannot be hardened by heat treatment. They contain between 10.5% to 27% of chromium and very little nickel. Most compositions include molybdenum; some, aluminium or titanium.

III. **Martensitic stainless steels:** These are not corrosion resistant as the other two classes, but are extremely strong and tough as well as highly machineable, and can be hardened by heat treatment. Martensitic stainless steel contains chromium (12-14%), molybdenum (0.2-1%), about 0.1-1% carbon and no nickel.

IV. **Precipitation - hardening martensitic stainless steels:** They have corrosion resistance comparable to that of austenitic varieties. It can be hardened by precipitation to even higher strengths than the other martensitic grades. It consist of about 17% chromium and 4% nickel.

V. **Duplex stainless steels:** They have a mixed microstructure of austenite and ferrite. The aim being to produce a 50:50 mix although in commercial alloys the mix may be 40:60 respectively. Duplex steel have improved strength over austenitic stainless steels and also improved resistance to localised corrosion particularly pitting, crevice corrosion and stress

corrosion cracking. They are characterized by high chromium (19-28%) and molybdenum (up to 5%) and lower nickel contents than austenitic stainless steels.

1.5. STAINLESS STEEL GRADES

- 200 Series- austenitic chromium-nickel-manganese alloys
- 300 Series- austenitic chromium-nickel alloys
    - Type 301- It is highly ductile and used for formed products. It hardens rapidly during mechanical working.
    - Type 303- It is the free machining version of 304 after addition of sulfur
    - Type 304- It is the most common steel (the classic 18/8 stainless steel).
    - Type 316- It is the next most common type after type 304. It is used for food and surgical stainless steel. Addition of molybdenum prevents specific forms of corrosion. It is also known as "marine grade" stainless steel due to its increased ability to resist saltwater corrosion compared to type 304. It is often used for building nuclear reprocessing plants.
- 400 Series- ferritic and martensitic chromium alloys
    - Type 408- It is heat-resistant and poorly corrosion resistance. It contains 11% chromium and 8% nickel.
    - Type 409- It is the cheapest type. It is used in automobile exhausts. It contains ferritic (iron/chromium only).
    - Type 410- Martensitic (high-strength iron/chromium).
    - Type 420- It is “cutlery grade” martensitic which is similar to the Brearley's original "rust less steel". It is also known as "surgical steel".
    - Type 430- Decorative, e.g., for automotive trim; ferritic.
    - Type 440- It is used in a higher grade of cutlery steel, which contains more carbon in it. To allow for much better edge retention when the steel is heat treated properly.
- 500 Series- Heat resisting chromium alloys
- 600 Series- Martensitic precipitation hardening alloys
    - Type 630- It is the most common stainless steel, better known as 17/4. It contains 17% chromium and 4% nickel

1.6. APPLICATION OF STAINLESS STEEL

Lower alloyed grades resist corrosion by the atmospheric and pure water environments, while high-alloyed grades can resist corrosion by most acids, alkaline solutions, and chlorine bearing environments: a properties which are utilized in process plants. Special high chromium and nickel-alloyed grades has the fire and heat resistive properties. It resist scaling and retain strength at high temperatures. The easy cleaning ability of stainless makes it the first choice for strict hygiene conditions, such as hospitals, kitchens, abattoirs and other food processing plants. The work-hardening property of austenitic grades, results in significant strengthening of the material from cold-working. The high strength duplex grades, allow reduced material thickness over conventional grades, therefore it is cost saving.

1.7. GAS TUNGSTEN ARC WELDING

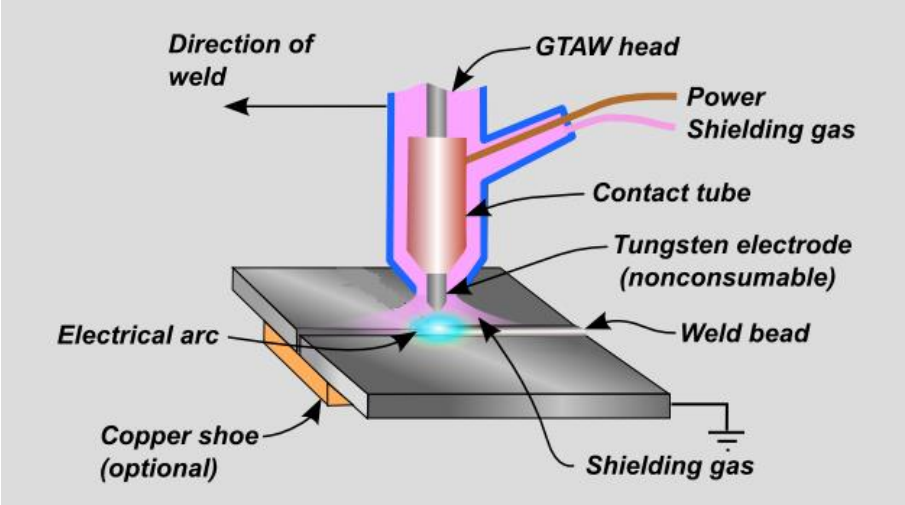

Figure 1. 1: GTAW welding Process

Gas tungsten arc welding (GTAW), commonly known as tungsten inert gas (TIG) welding, is an arc welding process that uses a non-consumable tungsten electrode to produce the weld. The weld area is protected from atmospheric contamination by a shielding gas (usually an inert gas such as argon), and a filler metal is normally used. GTAW is most commonly used to weld thin sections of stainless steel and light metals such as aluminum, magnesium, and copper alloys.

CHAPTER 2

REVIEW OF LITERATURE

2.1. INTRODUCTION

Welding of dissimilar metals has been the objective of investigation for many years; their growing importance is justified by their technical, economic potential and the beneficial properties of two metals [1,2]. Copper and its alloys have been widely used in aerospace, micro-electronics and metallurgy fields due to their excellent properties such as high thermal conductivity and good ductility [3]. However, the application of copper and its alloy is limited due to its high density and cost. While stainless steel is a common material with low cost in most industry [4,5].

However, one of the main problems for copper and stainless steel welding is their great differences between melting temperature and thermal conductivity. Asymmetrical temperature field will be formed during the welding process. As a result, the grain on the copper side always grows coarse. Another major problem in copper and stainless steel welding is hot cracking in the heat-affected zone (HAZ) of stainless steel due to copper penetration into grain boundaries of steel [6]. In order to overcome the above problems, copper alloy and stainless steel have been welded by several methods such as arc welding, diffusion bonding, brazing, laser beam welding and electron beam welding. In this chapter the different methods for welding of dissimilar metals has been reviewed and special emphasis has given to weld copper and stainless steel. This chapter also reviews the different characteristics of copper and stainless steel welding with respect to tensile strength, microstructure and microhardness.

2.2. LITRATURE REVIEW

M. Velu et al. (2015) investigated experimentally the fracture toughness and fatigue crack growth behaviour of mode-I cracked bi-metallic compact tension specimens. The specimens were made of weak-copper (UNSC11000) and strong-alloy steel (En31) and arc-welded with nickel-filler. Residual stresses induced in constituent materials during welding, due to their different coefficients of thermal expansion (thermal mismatch) were measured at important locations in all the materials near the weld zone. Thermal and mechanical mismatches between constituent materials, were strongly found to affect the behavior of crack tip in the vicinity of the weld under

both monotonic and fatigue load. The results also reported in this paper revealed that Cu-steel joint arc welded with nickel-filler appears to be suitable for application under larger monotonic and cyclic-mechanical loads and primarily attributed to good weld-quality by use of nickel-filler.**[7]**

R. Kumar et al. (2015) Studied the friction welding characteristics between Ti-6Al-4V and SS304L into which pure oxygen free copper (OFC) was introduced as interlayer and without interlayer. Box-Behnken design was used to minimize the number of experiments to be performed. The weld joint was analyzed for its mechanical strength. The study revealed that the highest tensile strength between Ti-6Al-4V and SS304L between which pure copper was used as insert metal was acquired. It was found that copper as interlayer has produced high tensile strength in the order of 523.6 MPa as compared to the joints established without interlayer. It was also observed that the samples with minimum interlayer thickness have produced better results. **[8]**

Bing-Gang Zhang et al. (2014) performed electron beam welding (EBW) of 304 stainless steel to QCr0.8 copper alloy with copper filler wire. Orthogonal experiment was performed to investigate the effects of process parameters on the tensile strength of the joints, and the process parameters were optimized. The optimum process parameters were as follows: beam current of 30 mA, welding speed of 100 mm/min, wire feed rate of 1 m/min and beam offset of −0.3 mm. The microstructures of the optimum joint were studied. The results indicated that the weld is mainly composed of dendritic α phase with little globular ε phase, and copper inhomogeneity only occurs at the top of the fusion zone. In addition, a melted region without mixing exists near the weld junction of copper side. This region with a coarser grain size is the weakest section of the joints. It was also found that the microhardness of the weld decreases with the increase of the copper content in solid solution. The highest tensile strength of the joint was found to be 276 MPa.**[9]**

Y. Kchaou et al. (2014) investigated the Shielded Metal Arc Welding (SMAW) on UNS N08028 (Alloy 28) super austenitic stainless steel sheets. The author investigated the microstructure and the mechanical properties of base metal (BM), weld metal (WM), and welded joint (WJ). Optical micrographs showed that the base metal presents austenitic grains, and the weld metal exhibits a fully austenitic dendritic structure, confirming the Schaeffler diagram estimations. Microhardness

measurements indicated that the hardness increased in the weld bead due to the rapid cooling and thermal cycle during welding procedure. The measured mechanical properties and the analysis of the fracture profiles showed that the two materials were ductile but the ductility was less pronounced in the weld metal. Consistently the yield stress, the plastic strength and the impact toughness were lower than in the base metal. In addition, the BM presents a higher cyclic hardening and plastic strain compared to those of WM. Cyclic stress–strain hysteresis loops shows that WM and WJ have almost the same cyclic behavior, especially at high imposed strain levels.**[10]**

M.A. García-Renteríaa et al. (2014) Studied the resistance to localized corrosion of AISI 2205 duplex stainless steel plates joined by Gas Metal Arc Welding (GMAW) under the effect of electromagnetic interaction of low intensity (EMILI) with sensitive electrochemical methods. Welds were made using two shielding gas mixtures: 98% Ar + 2%O_2(M1) and 97% Ar + 3% N2(M2). Plates were welded under EMILI using the M1 gas with constant welding parameters. The modified microstructural evolution in the high temperature heat affected zone and at the fusion zone induced by application of EMILI during welding was associated with the increase of resistance to localized corrosion of the welded joints. Joints made by GMAW using the shielding gas M2 without the application of magnetic field presented high resistance to general corrosion but high susceptibility to undergo localized attack.**[11]**

K. Devendranath Ramkumar et al. (2014) investigates the weldability, metallurgical and mechanical properties of the UNS 32750 super duplex stainless steels joints by Gas Tungsten Arc Welding (GTAW) employing ER2553 and ERNiCrMo-4 filler metals. Impact and tensile studies investigated that the weldments employing ER2553 exhibited superior mechanical properties compared to ERNiCrMo-4 weldments. Microstructure studies performed using optical and SEM analysis clearly exhibited the different forms of austenite including widmanstatten austenite on the weld zone employing ER2553 filler. Also the presented results clearly reported the effect of filler metals on strength and toughness during the multi-pass welding. This research article addressed the improvement of tensile and impact strength using appropriate filler wire without obtaining any deleterious phases.**[12]**

Z.H. Liu et al. (2014) studied the separation of two different materials within a single dispensing coating system by Multi-material processing in selective laser melting using a novel approach. The 316L stainless steel and UNS C18400 Cu alloy multi-material samples were produced using selective laser melting and their interfacial characteristics were analyzed using focused ion beam, scanning electron microscopy, energy dispersive spectroscopy and electron back scattered diffraction techniques. A substantial amount of Fe and Cu element diffusion were observed at the bond interface suggesting good metallurgical bonding. Quantitative evidence of good bonding at the interface was also obtained from the tensile tests where the fracture was initiated at the copper region. The tensile strength of steel/Cu SLM parts was evaluated to be 310 ± 18 MPa and the variation in microhardness values was found to be gradual along the bonding interface from the steel region (256 ± 7 $HV_{0.1}$) to the copper region (72 ± 3 $HV_{0.1}$).**[13]**

M. Velu et al. (2013) showed that the metallurgical and mechanical examinations of joints between dissimilar metals like UNSC 11000 (copper) and alloy steel (En31). This was obtained by Shielded Metal Arc Welding (SMAW) using two different filler materials; bronze and nickel-base super alloy. While Weld bead of the joint with nickel-filler did not display porosity, the weld bead of the joint with bronze-filler did. In tension tests, the weldments with bronze-filler was seen to have fractured in the center of the weld, while those with nickel-filler fractured in the heat affected zone (HAZ) of copper. Since the latter exhibited higher strength than the former, all the major tests were undertaken over the joints with nickel-filler alone. Scanning Electron Microscopy (SEM) coupled with Energy Dispersive Spectroscopy (EDS) indicated corrugated weld interfaces and favorable elemental diffusions across them. X-ray diffraction (XRD) studies around the weld interfaces did not reveal any detrimental intermetallic compounds. Transverse bending tests however showed that flexural strengths of the weldments were higher than the tensile strengths. Transverse side bend tests confirmed good ductility of the joints. Shear strength of the weld-interface (Cu–Ni or Ni–steel) was higher than the yield strength of weaker metal. **[14]**

Ting Wang et al. (2013) designed composite V/Cu based filler metals for electron beam welding of titanium stainless steel joint, based on the element metallurgical compatibility. Powder metallurgy method had been applied to manufacture the filler metal. To determine the feasibility

of these filler metals, microstructures were analyzed by optical microscopy, scanning electron microscopy and X-ray diffraction. Mechanical properties of the joints were evaluated by tensile strength tests. The feasibility of the Cu/V filler metal was poor due to the differences in physical properties between copper and vanadium, vanadium and titanium. A non-fusion defect was produced in the joint under low heat input, and cracking occurred in the joint under higher heat input due to the continuously distributed brittle TiCu, TiFe and τ_2 compounds. However, such defects were eliminated using a powder metallurgical V/CueV filler metal. A joint with a tensile strength of 395 MPa, 72% of that of the stainless steel was obtained. And almost no intermetallic were detected in Ti/V/Cu-V/Fe joint.**[15]**

R. Mendes et al. (2013) studied the influence of explosive characteristics on the weld interfaces of stainless steel AISI 304L to low alloy steel 51CrV4 in a cylindrical configuration. The effect of ammonium nitrate-based emulsion, sensitized with different quantities and types of sensitizing agents (hollow glass microballoons or expanded polystyrene spheres) and Ammonium Nitrate Fuel Oil (ANFO) explosives on the interface characteristics was analyzed. The study showed that the type of explosive and the type and proportion of explosive sensitizers affected the main welding parameters, and particularly collision point velocity. The morphology of the wavy weld interfaces, chiefly the amplitude and length of the waves, was affected both by the impact velocity and the type and particle size of the explosive sensitizers, and increased with particle size. All the weld interfaces, except welds done with ANFO, displayed localized melted and solidified regions, whose chemical composition resulted from the contribution of both flyer and base metal.**[16]**

Shuhai Chen et al. (2013) done the laser butt welding of titanium alloy to stainless steel. The effect of laser-beam offsetting on microstructural characteristics and fracture behavior of the joint was investigated. More durable joint was found when the laser beam was offset towards the stainless steel side. The intermetallic compounds have a uniform thickness along the interface and were divided into two layers. One consisted of FeTi + α-Ti, and other consisted of FeTi + Fe_2Ti + $Ti_5Fe_{17}Cr_5$. When laser beam was offset by 0 mm and 0.3 mm toward the titanium alloy side, the joints fracture spontaneously after welding. However, durable joining was achieved only when the laser beam is offset by 0.6 mm toward the titanium alloy. From the top to the bottom of the joint, the thickness of intermetallic compounds continuously decreased and the following interfacial

structures were found: FeAl + α-Ti/Fe_2Ti + $Ti_5Fe_{17}Cr_5$, FeAl + α-Ti/FeTi + Fe_2Ti + $Ti_5Fe_{17}Cr_5$ and FeAl + α-Ti, in that order. The tensile strength of the joint was higher when the laser beam was offset toward the stainless steel than toward the titanium alloy, with the highest observed value being 150 MPa. It was also seen that the fracture on the joint occurs along the interface between two adjacent intermetallic layers.**[17]**

I . Tomashchuk et al. (2013) studied the influence of operational parameters on the local phase composition and mechanical stability of the electron beam welds between titanium alloy and AISI316L austenitic stainless steel with a copper foil as an intermediate layer. The study also revealed that two types of weld morphologies could be obtained depending on beam off set from the center line. Beam shift toward the titanium alloy side results in formation of a large amount of the brittle TiFe2 phase, which is located at the steel/melted zone interface and leads to reducing the mechanical resistance of the weld. Beam shift toward the steel side inhibits the melting of titanium alloy and, so, the formation of brittle intermetallics at the titanium alloy/melted zone interface. Mechanical stability of the obtained junctions were shown to depend on the thickness of this intermetallic layer. The fracture zone of the weld were found to beam mixture of TiCu (3–42 wt%), TiCu1_xFex (x¼0.72–0.84) (22– 68wt%)and TiCu1_xFex (x¼0.09–0.034) (0–22 wt.**[18]**

Shuhai Chen et al. (2013) revealed the microstructures and its formation mechanism of formation of a stainless steel/copper dissimilar joint by laser welding. It was found that the two modes of joining, i.e., welding-brazing and fusion welding, depend on different processing parameters. In the welding-brazing mode, the interface between copper and the fusion zone had scraggy morphology because the molten pool is frozen by solid copper with high thermal conductivity. The inter diffusion of elements occurred in the neighborhood of the interface, which lead to the metallurgy bond of the mode. In the fusion welding mode, the liquid phase in the fusion zone undergoes not only primary but also secondary liquid separation due to the high cooling rate and high super cooling level of laser welding. Some micro cracks generated in the fusion zone by thermal stress mismatch are healed by liquid copper filling.**[19]**

Mallaiah Gurram et al. (2012) showed the influence of grain refining elements such as copper (Cu) and aluminium (Al) on mechanical properties of AISI 430 ferritic stainless steel welds

through gas tungsten arc welding process. Cu (foil form) and Al powder of -100 um mesh was added in the range from 1 to 3 g between the butt joint of ferritic stainless steel. In order to investigate the influence of post-weld heat treatment on the microstructure and mechanical properties of welds, post-weld annealing was adopted at 830^{o} C, with 30 min holding followed by water quenching. Besides that corrosion, behavior of ferritic stainless steel welds were also studied. From this investigation, it was observed that the joints made by the addition of 2 g Al (2.4 wt.%) in post weld annealed condition led to an improvement in the strength. There was a marginal enhancement in the ductility and pitting corrosion resistance of ferritic stainless steel welds by the addition of 2 g Cu (0.18 wt.%) in post-weld annealed condition. The observed mechanical properties had been correlated with microstructure, fracture features and corrosion behaviour of ferritic stainless steel weldments.**[20]**

Bina Mohammad Hosein et al. (2013) studied explosive welding and heat treatment processes provided an effective method for manufacturing high-strength and high-ductility copper/ austenitic stainless steel couple. In order to improve diffusion in the interface of copper/stainless steel, first the tensile samples were provided from the welded part, then they were subjected to annealing at 300^{o} C (below recrystallization temperature) for 8–32 h with 8 h intervals and then samples were cooled in the furnace. Optical microscopy (OM), scanning electron microscopy (SEM) and energy dispersive spectroscopy (EDS) were utilized to evaluate the possibility of diffusion in the joints. Moreover, in order to measure the hardness of the samples, microhardness test were performed. Microstructural evaluations showed that the stainless steel 304L had a wavy interface. The post heat treatment process resulted in great enhancement of diffusion. Microhardness measurements showed that the hardness of the sample near to the interface was greatly higher than other parts; this is the result of plastic deformation and work hardening of copper and stainless steel 304L in these regions.**[21]**

Sajjad Gholami Shiri et al. (2012) welded CP-copper to 304 stainless steel by gas tungsten arc welding process using different filler materials. They tried to show that the formation of defect free joint by using copper filler material. But, the presence of some defects like solidification crack and lack of fusion caused deterioration in the tensile strength of other joints. In the optimum conditions, the tensile strength of the joint was 96% of the weaker material. Also, this joint was

bent to 180º without any macroscopic defects like separation, tearing or fracture. It was then concluded that copper is a new and good candidate for gas tungsten arc welding of copper to 304 stainless steel.**[22]**

Ting Wang et al. (2010) Showed electron beam welding of Ti-15-3 titanium alloy to 304 stainless steel with a copper sheet as interlayer. Microstructures of the joint were studied by optical microscopy (OM), scanning electron microscopy (SEM) and X-ray diffractometry (XRD). In addition, the mechanical properties of the joint were evaluated by tensile test and the microhardness was measured. These two alloys were successfully welded by adding copper transition layer into the weld. Solid solution with a certain thickness was located at the interfaces between weld and base metal in both sides. Regions inside the weld and near the stainless steel were characterized by solid solution of copper with TiFe2 intermetallics dispersedly distributed in it. The hardness of the weld came to the highest value when it contained Ti-Cu and Ti-Fe-Cu intermetallic layer near titanium alloy.**[23]**

J.J. del Coz Díaz et al. (2010) performed thermal stress analyses in tungsten inert gas (TIG) welding process of two different stainless steel specimens in order to compare their distortion mode and magnitude. The growing presence of non-conventional stainless steel species like duplex family generates uncertainty about how their material properties could be affected under the welding process. To develop suitable welding numerical models, authors considered the welding process parameters, geometrical constraints, material non-linearity's and all physical phenomena involved in welding, both thermal and structural. Four different premises were taken into account. Firstly, all finite elements corresponding to the deposition welding are deactivated and, next, they were reactivated according to the torch's movement to simulate mass addition from the filler metal into the weld pool. Secondly, the movement of the TIG torch was modelled in a discontinuous way assuming a constant welding speed. Thirdly, the arc heat input were applied to the weld zone using volumetric heat flux distribution functions. Fourthly, the evolution of the structural response were tackled through a stepwise non-linear coupled analysis. The numerical simulations were validated by means of full-scale experimental welding tests on stainless steel plates **[24].**

D Liang et al. (2010) Showed Ni–Cu–Pd welding consumables have been recently developed for 300-series austenitic stainless steels such as Type 304L (SS304L) to reduce the amount of Cr(VI) in the welding fumes. In this study, a modified filler metal that replaced Pd with Ru was evaluated. Initial tests conducted on button-melted samples and bead-on-plate welds indicated that Ni–Cu–Ru exhibited good corrosion properties. Actual Ni–Cu–Ru arc welds made on SS304L were successfully produced and the corrosion performance was comparable to or better than that of Ni–Cu–Pd welds. These welds are a suitable replacement for welds made with standard 300-series welding consumables, such as SS308L **[25].**

M. Weigl et al. (2010) presented the laser-welding of copper and stainless steel connections for applications in power electronics. The particular demand for such dissimilar connections was caused by the increasing implementation of electronics in areas with contact to corrosive fluids, which copper cannot resist. The influence of a lateral displacement of the laser beam and the feed rate on the metallurgical properties of the dissimilar materials connection was studied and the effects of these parameters were discussed on the base of metallographic specimen, micro-hardness measurements and element analysis **[26]**.

J.L. Song, S.B. Lin, C.L. Yang, G.C. Ma, H. Liu (2009) studied the welding of dissimilar metals by TIG welding–brazing of 5A06 aluminum alloy to SUS321 stainless steel using 4047 Al–Si eutectic filler metal and modified non-corrosive flux. And spreading behavior of filler metal on the groove surface and microstructure characteristics of the butt joint were investigated. The spreading behavior of liquid filler metal consisted of two parts: one was to spread on the back face to pack the steel; the other was to uphill spread on the front face of the groove to form a sound brazed seam. This paper reported that tensile strength of the butt joint reached 120.0MPa and fracture occurred at the interfacial layer. Cracks derived from the top part of brittle η-Fe_2Al_5 interfacial layer when its thickness exceeded 100μm **[27]**.

2.3. GAPS IN LITRATURE REVIEW

The literature survey revealed that plasma arc welding, friction stir welding, electron beam welding, shielded metal arc welding, gas welding and laser welding are the different method to

weld dissimilar metal. A limited work has been reported on GTAW [13,24] and specially to weld copper with stainless steel because of great difference between melting temperature and thermal conductivity which causes asymmetrical temperature field formed during welding process. For this reason welding of copper and stainless steel by GTAW method has been selected and studied.

2.4. MOTIVATION AND OBJECTIVE

The motivation of this project was to study the GTAW process in its totality and to explore the potential of controlling the process so as to get desired output by simply manipulating the input process variables. The objective of the project was to weld copper with stainless steel using brass as filler material by gas tungsten arc welding, to find the effect of welding parameters such as current, gas flow rate, offset and speed on the weldment and to investigate the tensile strength, microstructure, micro hardness of the weldment.

CHAPTER 3

THEORY

3.1.INTRODUCTION

Gas tungsten arc welding (GTAW) is commonly known as tungsten inert gas (TIG) welding. It is an arc welding process. Which uses a non-consumable tungsten electrode, to produce the weld. A shielding gas (usually an inert gas such as argon) is used to protect the weld from atmospheric contamination. A filler metal is usually used but some welds which are known as autogenous welds do not require a filler metal. GTAW process was followed to weld two dissimilar metal the details of which are given below.

3.2. GAS TUNGSTEN ARC WELDING EQUIPMENT

In gas tungsten arc welding the equipment that are required for the operation are a constant-current welding power supply a welding torch having a non-consumable tungsten electrode and a gas source (Figure 3.1).

Figure 3. 1: Gas Tungsten Arc Welding Torch

3.2.1. Welding torch

Gas tungsten arc welding torches are designed for either automatic or manual operation. They are also equipped with cooling systems using air or water. Torches may be automatic or manual but are similar in construction. The manual torch has a handle while the automatic torch normally comes with a mounting rack. The angle between the centerline of the handle and the centerline of the tungsten electrode is known as the head angle. This can be changed in some manual torches according to the preference of the operator. Air cooling systems are most often used for low-current operations (up to about 200 A), while water cooling is required for high-current welding (up to about 600 A). The torches are connected with cables to the power supply and with hoses to the shielding gas source and where used, the water supply.

Figure 3. 2: Gas Tungsten Arc Welding Torch

The internal metal parts of a torch are made of hard alloys of copper or brass in order to transmit current and heat effectively. The tungsten electrode must be held firmly in the center of the torch with an appropriately sized collet, and ports around the electrode provide a constant flow of shielding gas. The body of the torch is made of heat-resistant, insulating plastics covering the metal components, providing insulation from heat and electricity to protect the welder.

The size of the welding torch nozzle depends on the size of the desired welding arc, and the inside diameter of the nozzle is normally at least three times the diameter of the electrode. The nozzle must be heat resistant and thus is normally made of alumina or a ceramic material, but fused quartz, a glass-like substance, offers greater visibility. Devices can be inserted into the nozzle for special applications, such as gas lenses or valves to control shielding gas flow and switches to control welding current.

3.2.2. Power supply

There are three basic power supplies used in the TIG welding process. They are a direct current straight polarity (DCSP) power supply; the direct current reverse polarity (DCRP) power supply, and the alternating current high frequency (ACHF) modified power supply. In the DCSP power

Figure 3. 3: Gas Tungsten Arc Welding Power Supply

supply, the tungsten electrode is negative or the cathode, and the base metal is positive or the anode. The electron flow is from the cathode to the anode. Because of the direction of this flow approx. two-third of the total heat in the arc column, which is approx. 11000 F, is released in the

base metal. The tungsten electrode, then, can be of a very small diameter because the tungsten will not receive the major portion of the heat. It can have a smaller mass to dissipate the heat that it can absorb.

The positive ions flow from the base metal to the tungsten electrode. When they strike the electrode, a small amount of heat is released. The positive ions strike molecules in the atmosphere, creating an ionization layer of gas or an ionized gas, which protects the major electron flow as in shield arc welding. The DCSP power supply does not perform any cleaning action; therefore, the base metal must be cleaned in order to use DCSP.

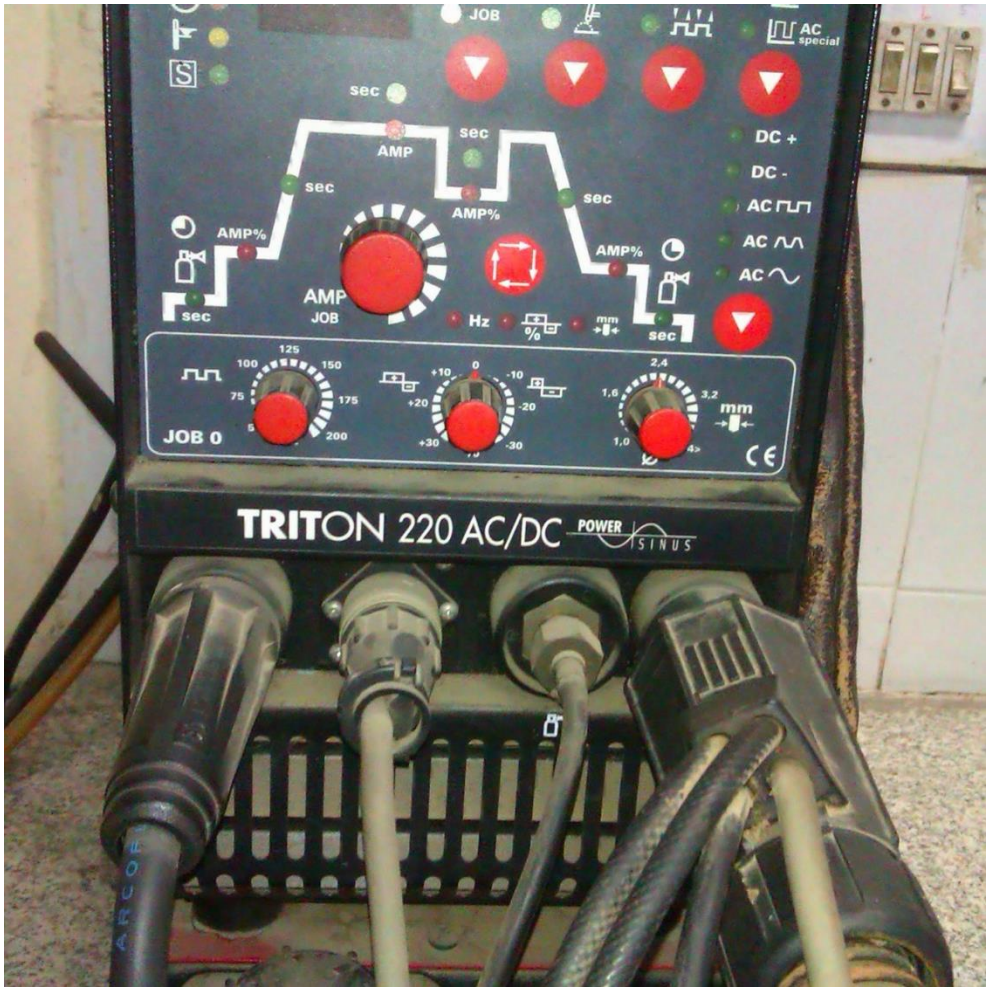

Figure 3. 4: Power Supply control panel

In the DCRP power supply, the electron flow is from the base metal, or work piece, to the electrode. Because of this electron flow to the tungsten electrode, approx. two-third of the heat generated by the arc column is absorbed by the tungsten electrode, which places a requirement for a larger mass upon the electrode. The minimum diameter of the electrode mass is thought to be ¼ inch so that it

can absorb excess heat. The electrons that leave the base metal and are accelerated towards the electrode carry with them some of the oxides that protect the surface of the metal, especially in case of aluminum. The cleaning of the oxide film results from the bombardment of the surface by the positively charged ions, which are thought to cause an electronic disassociation of the surface oxide from the metal, and by the explosion of the electrons off the base metal, through the oxide film, towards the anode electrode.

There are basically three kinds of tungsten or tungsten alloys that are used for the electrode in TIG welding: pure tungsten, zirconiated tungsten, and thoriated tungsten. Pure tungsten has a melting point of approximately 6170 F and a boiling point of 10,706 F, which gives the tungsten electrode a long life. Tungsten is also an excellent thermo ionic metal, or a metal that releases electrons extremely well at elevated temperature. However, slight modification of tungsten can improve the thermion emission of electrons, which helps the starting of the arc column because the improvement results in an easier release of electrons from the tungsten alloy. Thorium or zirconium is alloyed with the tungsten in small amounts, ranging form 2% down to 0.001 percent of the alloying ingredient. Thorium has a melting point of 3182 F, and zirconium a melting point of 3366 F. although there is a decrease in the melting point from the pure tungsten, the improvement in the thermo ionic emission of electrons aids in maintaining the life of electrode. The mass of the electrode also helps to keep the electrode form melting, as does the inert gas surrounding the tungsten electrode, which cools it. The tip of the tungsten electrode is the only part that becomes molten. Generally, a molten droplet is formed at the end of the electrode, especially in the DCRP. With alternating current, the small ball-shaped molten droplet most definitely forms at the end of the tungsten electrode. The initial shape of the tungsten electrode can either aid or hinder the thermo ionic emission of electrons from the tungsten electrode. With DCSP, the tip should be ground into a conical shape. With DCRP, the tip should be ground into a conical shape but with a blunted end. With alternating current, the tip should be rounded slightly. The current passing through the tungsten electrode and the melting of the tip of the electrode slightly change the shape. With DCRP, a small ball forms at the end of the electrode, and with alternating current, a large ball forms. However, with DCSP, the tip pretty much maintains its shape.

3.2.3. Electrode

The electrode used in GTAW is made of tungsten or a tungsten alloy, because tungsten has the highest melting temperature among metals, at 3422 °C. As a result, the electrode is not consumed during welding, though some erosion (called burn-off) can occur. Electrodes can have either a clean finish or a ground finish—clean finish electrodes have been chemically cleaned, while ground finish electrodes have been ground to a uniform size and have a polished surface, making them optimal for heat conduction. The diameter of the electrode can vary between 0.5 mm and 6.4 mm (0.02-0.25 in), and their length can range from 75 to 610 mm (3-24 in).

Figure 3. 5: Tungsten non consumable electrode

3.2.4. Tip shape

The arc performance depends, to a great extent on the shape of the electrode tip. Electrons jump more easily from a pointed tip than a blunt tip. Moreover, the arc is more directional and is slightly

stiffer when it comes off the end of a pointed electrode. Many welding procedures call for a specific tip shape. Tungsten electrodes are very sensitive to contamination. We should never use a general purpose grinding wheel to shape a tungsten tip, for the wheel will leave specks of other metals on the electrode. Tungsten electrodes should be prepared on a grinding wheel used exclusively for them. We should always grind the tip in a lengthwise direction. Do not hold the electrode at a right angle to the grinding wheel. The direction of the grinding marks helps to keep contaminating materials from sticking to the electrode. Tungsten electrodes are so sensitive to contamination that sometimes oil and sweat from fingers will change the arc.

3.3. WELDING PARAMETERS

In the study of welding of dissimilar metals by GTAW we considered the variation of following parameters:

3.3.1. Welding current (I)

Welding current is the most influential variable in TIG welding. It controls the depth of fusion and the amount of base metal fused. Welds made at excessively low current will tend to have little penetration and higher width - to depth ratio. Welds made at an excessively high current will have deep penetration, high dilution more shrinkage and excess build up. Low current will produce a less stable arc than higher currents.

The direction of current flow will also affect the weld bead profile. The current may be direct with electrode positive (reverse polarity), electrode negative (straight polarity) or alternating. Reverse polarity is the most commonly used. For a given set of welding conditions reverse polarity will produce wider beads with more penetration at a lower deposition rate than straight polarity. Straight - polarity welding will contribute to narrower beads with less penetration and more build up. Straight polarity is preferred for poor fit up. The bead shape penetration and deposition rate for alternating current fall between those of straight and reverse polarity.

3.3.2. Gas flow rates (G)

Argon gives a good, stable arc, is readily available, and is not as expensive as most of the others. Hydrogen, which was used for atomic hydrogen welding, has some basic problems. Hydrogen is flammable and lighter than air. Quite a bit of hydrogen is needed to give arc protection, and it burns with an invisible flame. Helium makes a very hot arc, which is more.

Figure 3. 6: Gas flow rate meter

3.3.3. Offset (O)

The difference in melting temperatures of copper and stainless steel that are to be joined must also be considered. This is of primary interest when a welding process utilizing heat is involved since one metal will be molten long before the other when subjected to the same heat source. When metals of different melting temperatures and thermal expansion rates are to be joined, the welding process with a high heat input that will make the weld quickly has an advantage. Owing to this we need to give an offset to the torch tip.

3.3.4. Speed (S)

As speed was taken as a parameter in welding. It was important to keep the speed of welding constant throughout the welding. So a bed was designed to keep the speed of welding constant. The bed in shown in figure 3.7.

Design was made, keeping in mind the slow speed that is required for TIG welding. For slow speed a lead screw was required, because a screw type motion can produce a very slow motion. In the design of the bed the bed was allowed to move between two parallel rods and the speed of the bed was controlled with the help of lead screw. The lead screw had 11 teeth per inch and the diameter of the lead screw 1.9 centimeter. 11 teeth per inch would produce a very small movement in the bed. The length of movement of the bed was 0.8 meter. And the length of the lead screw was also 0.8 m.

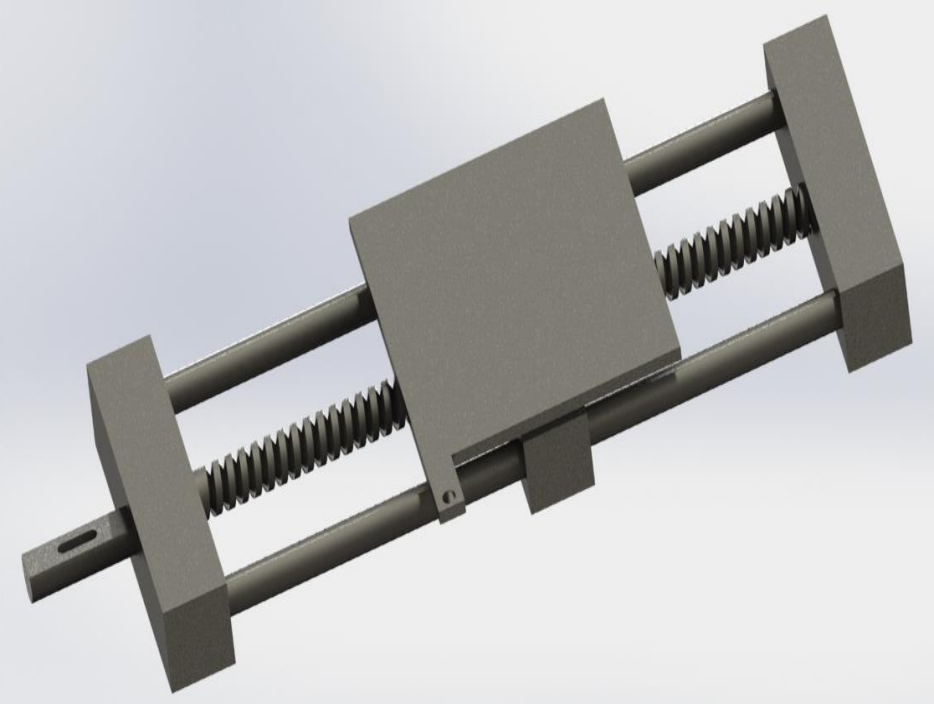

Figure 3. 7: Bed to control the speed

At the end of the lead screw a 5 speed sprocket was attached. Which would further reduce the speed of the bed. The sprocket not only reduced the speed it helped to even increase the speed when required. The sprocket was attached to the motor sprocket with the help of a chain. The chain gave it a slip free motion. The motor was a low rpm and high torque motor. High torque was required to make the lead screw rotate freely and so that it does not get jammed anywhere.

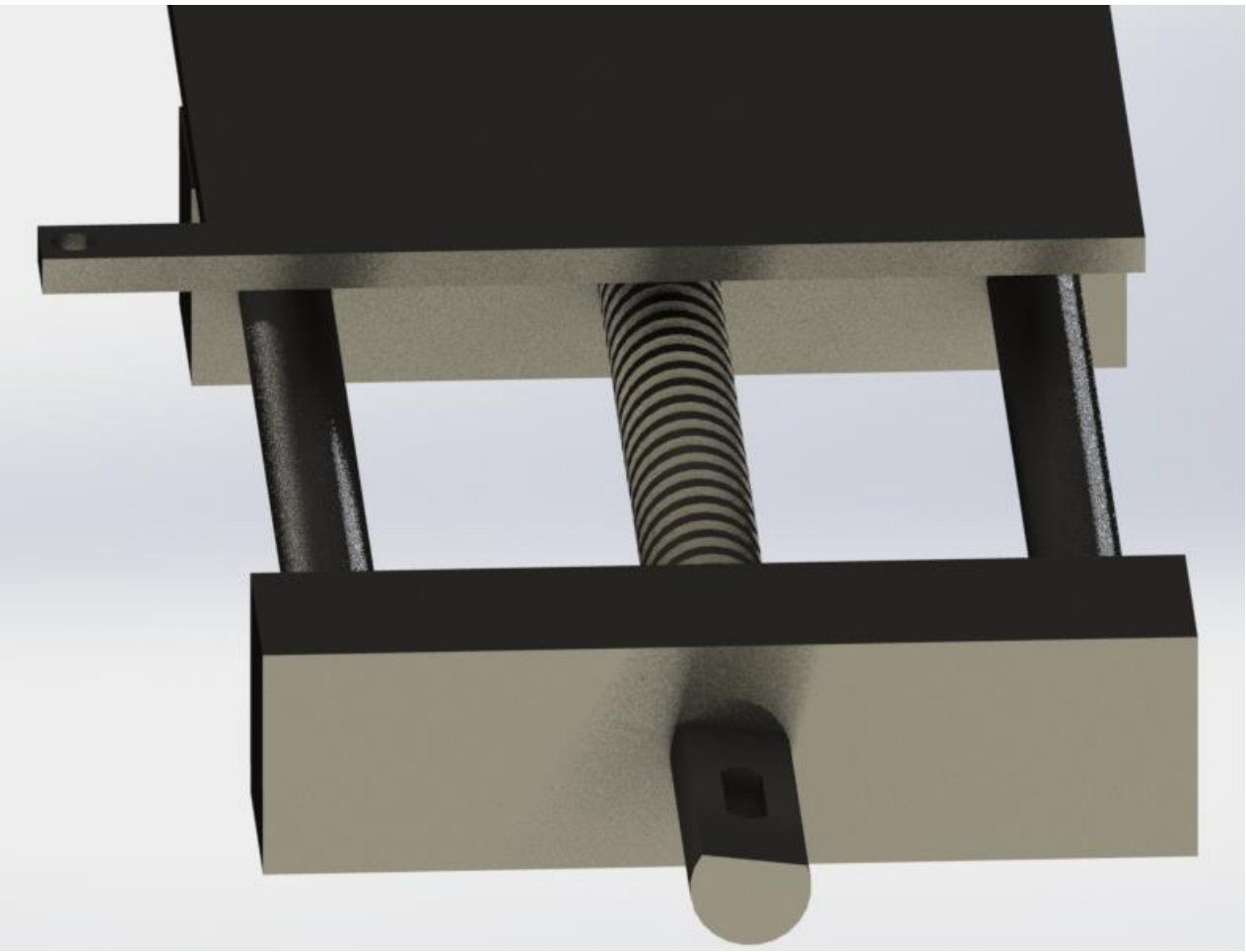

Figure 3. 8: Works on rack and pinion principle

3.4. ADVANTAGES OF GTAW PROCESS

The gas tungsten arc welding has several advantages. Tungsten Inert Gas Welding produces high quality welds. The weld is automatically protected by the inert gas during the welding process as the welding area is protected by argon or helium gas. In this type of welding there is no production of slag which makes it a cleaner weld. TIG Welding can be done in any position. The tungsten inert gas process can be used for welding aluminum, magnesium, stainless steel silicon bronze titanium, copper and copper alloy, and wide range of different metal thickness in mild steel. Top quality welds made in the above metal need little, if any, cleaning after welding period. TIG Welding is most often used for joining aluminum from 1/32 inch to 1/8 inch (0.79 to 3.2 mm) thick. Although heavier sections can be joined by TIG welding, other processes are usually more economical. TIG welding is an easy method of joining metals that are considered hard−to−weld,

and filler and base metals can be easily matched. With TIG welding, strip of scrap parent metal may be used for filler metal. Post−weld machining, grinding, or chipping can usually be eliminated due to the easily controlled weld reinforcement. The need for flux is eliminated, even on hard to weld metal such as aluminum.

3.5. APPLICATION OF GTAW PROCESS

GTAW can be used for depositing metals in all positions but the level of skill required is very high. It is extensively used without filler metal, for the welding of longitudinal seams of thin walled stainless steel and alloy steel pressure pipes and tubing's in continuous strip mills. In thick walled pipes the control of weld pool is important particularly for depositing the root runs. GTAW normally with filler metal, is often used for this purpose in pipework required for high pressure steam lines, power generating, chemicals and petroleum industries. Because GTAW is easily mechanized and gives high quality weld the process is quite popular for precision welding in the aircraft, atomic energy and instruments industries. Aircraft frames, jet engine casing and rocket motor case are typical examples of its use in aircraft industry. Circumferential and edge welds, for example, can sealing joints are very suitable for mechanized GTAW.

CHAPTER 4

DESIGN AND FABRICATION OF EXPERIMENTAL SETUP

The TIG welding process is carried out for welding the metal sheet of 1.5 mm thickness. Earlier this work was done manually. The reasons which were discussed are as follows,

1. Fumes produced by the tungsten electrode effects the health as well as the eyes
2. safety of the operator
3. Special purpose machines in the market are very expensive
4. To see the effect of speed as a parameter on the Ultimate Tensile Strength of the material
5. A constant speed cannot be obtained with a hand

4.1. DESIGN OF COMPONENT

4.1.1. Design of Translation Screw

Overall length = 90cm

Length of threaded portion = 80cm

Diameter = 2 cm

Calculation for lead Screw

Mass = 5 Kg

Force = 5 X 9.81 N(Kg m/sec^2)

= 49.05 N(Kg m/sec^2)

Torque = 49.05 × .01 Nm

= 0.49 Nm

Pitch $P = \frac{1}{n}$

$P = \frac{1}{11}$

= 0.09

Linear travel

Linear distance in one revolution of translation screw

$= \frac{24.5\ mm}{11\ \text{teeth/inch}}$

= 2.30 mm

DC Motor Speed = 1RPM

DC Motor Torque = .8Nm

Driving gear

No of Teeth = 20

Driven gear

1. No of Teeth = 28
2. No of Teeth = 24
3. No of Teeth = 20
4. No of Teeth = 16
5. No of Teeth = 14

Speed Ratio of the gear

N1 = No of teeth in Driving Gear

N2 = No of teeth in Driven Gear

S1 = Speed of Driving Gear (RPM)

S2 = Speed of driven Gear (RPM)

Case I

$N_1 \times S_1 = N_2 \times S_2$

$20 \times 1 = 28 \times S_2$

$S_2 = 0.714$ RPM

Linear Speed of the bed = S_2 × Linear travel

= 0.714 × 2.30

= 1.64 mm/min

Case II

$N_1 \times S_1 = N_3 \times S_3$

$20 \times 1 = 24 \times S_3$

$S_3 = 0.833$ RMP

Linear Speed of the bed = S_3 × Linear travel

= 0.833 × 2.30

= 1.91 mm/min

Case III

$N_1 \times S_1 = N_4 \times S_4$

$20 \times 1 = 20 \times S_4$

$S_4 = 1$ Rpm

Linear Speed of the bed = S_4 × Linear travel

= 1 × 2.30

= 2.3 mm/min

Case IV

$N_1 \times S_1 = N_5 \times S_5$

$20 \times 1 = 16 \times S_5$

$S_5 = 1.25$ RMP

Linear Speed of the bed = S_5 × Linear travel

= 1.25 × 2.30

= 2.87 mm/min

Case V

$N_1 \times S_1 = N_6 \times S_6$

$20 \times 1 = 14 \times S_6$

$S_6 = 1.42$ RMP

Linear Speed of the bed $= S_6 \times$ Linear travel

$= 1.42 \times 2.30$

$= 3.28$ mm/min

Constant speed bed:

To maintain a reasonable amount of control over the Speed, a constant speed bed was needed. We visualized and then designed the required jig on Solidworks which is a CAD software. After fine-tuning our design on Solidworks, then fabricated the bed which would maintain an accurate control over speed of welding.

The final assembly consists of many sub – assemblies and parts namely:

- Guide bar
- Lead screw
- Welding plate
- Bearings
- Bushes
- Movable block
- Work piece clamping system

The views of each part, sub-assembly and assembly are shown.

4.2. ASSEMBLY PARTS

4.2.1. Guide bar

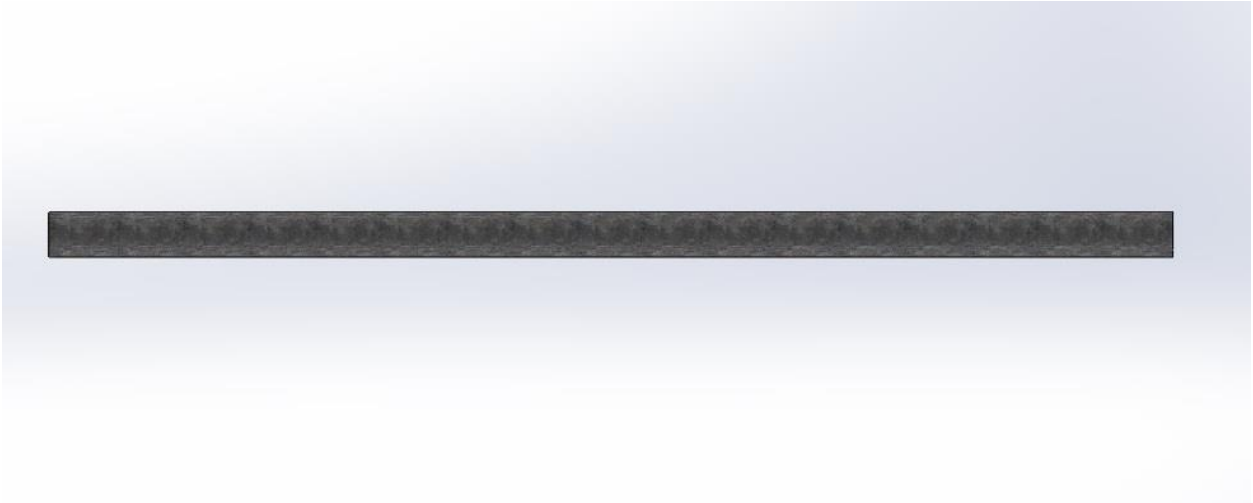

Figure 4. 1: Guide bar

- Length = 76.5 cm
- Diameter = 2 cm

4.2.2. Lead screw

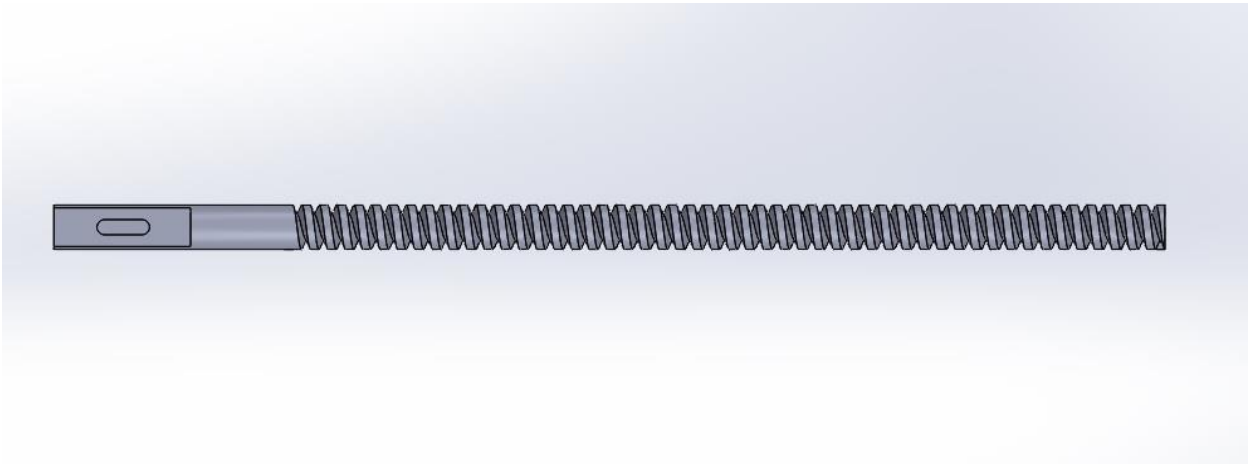

Figure 4. 2: Lead screw

- Length = 90 cm
- Diameter = 2 cm
- Teeth per inch = 11

4.2.3. End bar

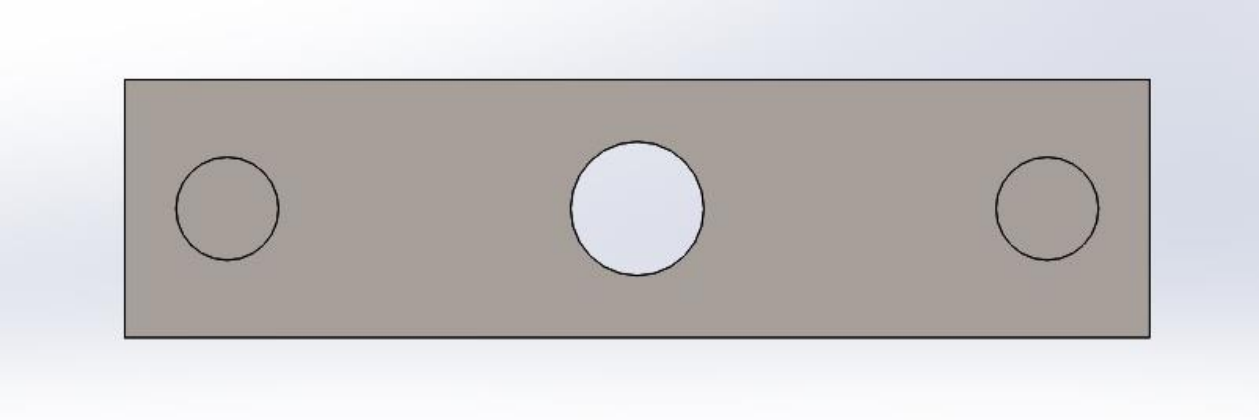

Figure 4. 3: Supporting end bar

- Length = 20 cm
- Breadth = 2 cm
- Height = 5 cm

4.2.4. Welding plate

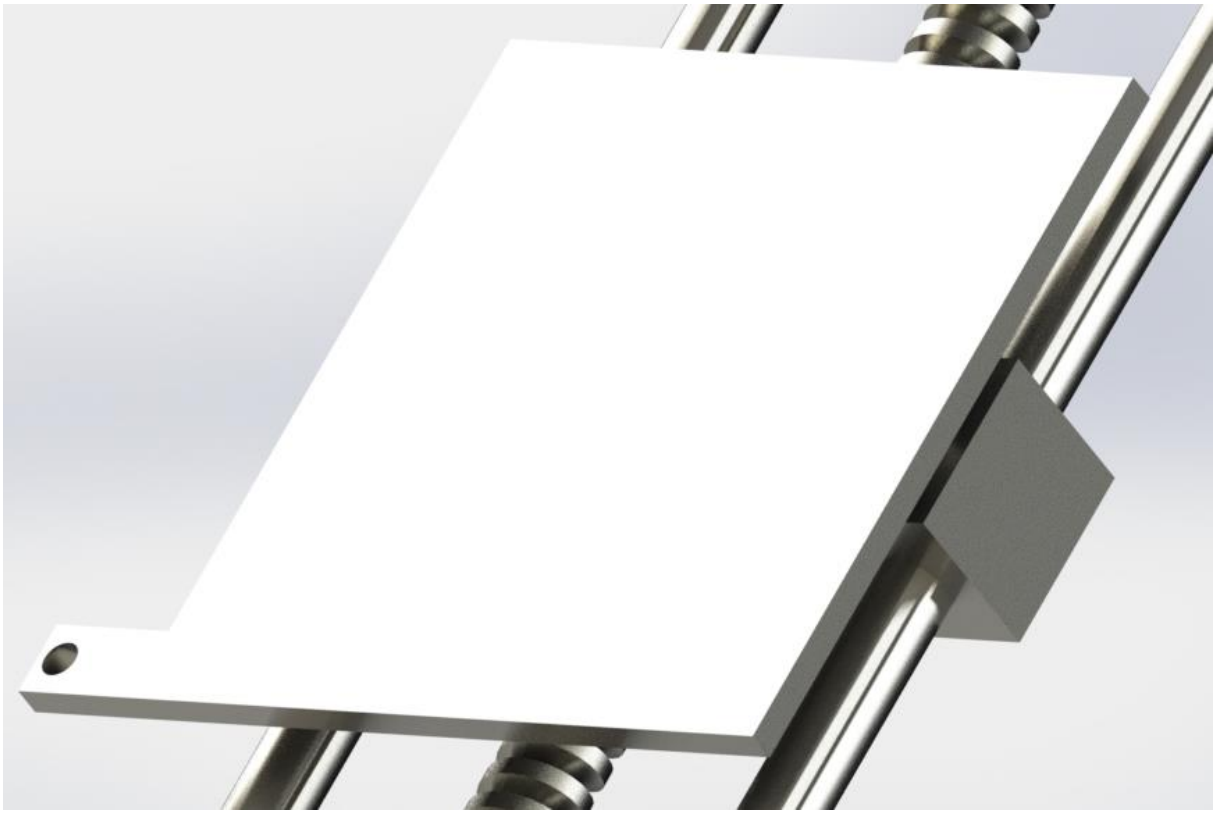

Figure 4. 4: Welding plate

4.2.5. Bearings

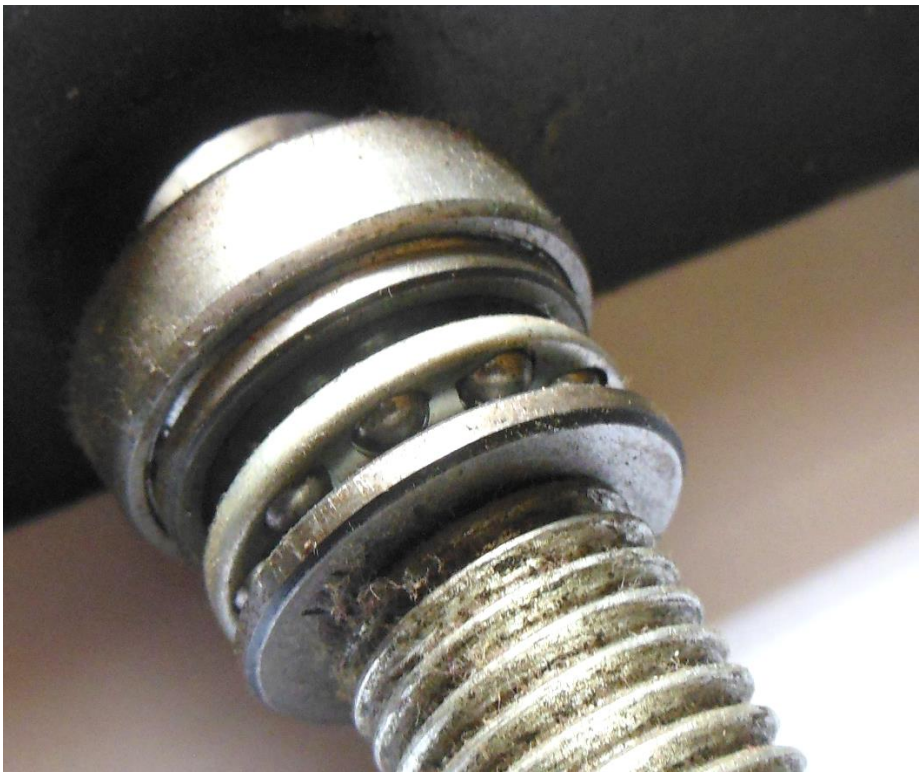

Figure 4. 5: Bearing to support the lead screw

4.2.6. Movable block

Figure 4. 6: Movable block for the welding plate

4.2.7. Work piece clamping system

During the welding stage, it was encountered that the two workpieces were separating midway in the welding process. To prevent this from happening, a designed was developed, which would hold the two strips together.

Figure 4. 7: Welding plate with work piece clamping strips

4.3. FULL ASSEMBLY

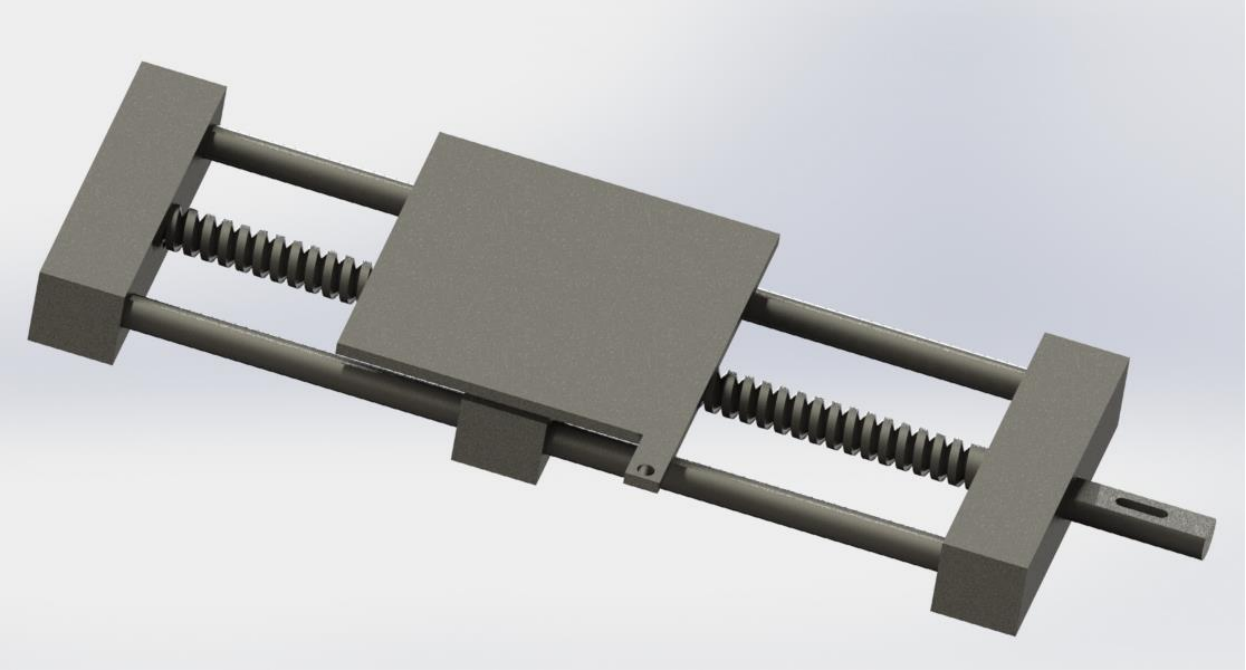

Figure 4. 8: Automate bed CAD model

Figure 4. 9: Automated bed

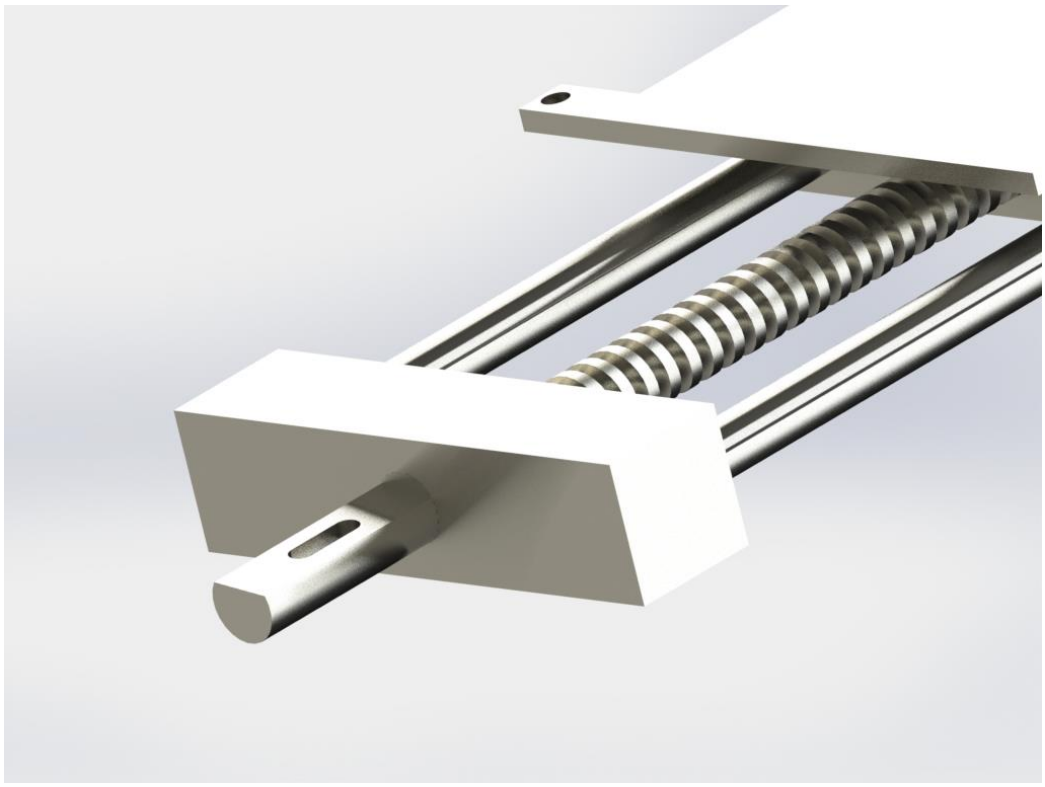

Figure 4. 10: CAD assembly of lead screw (front)

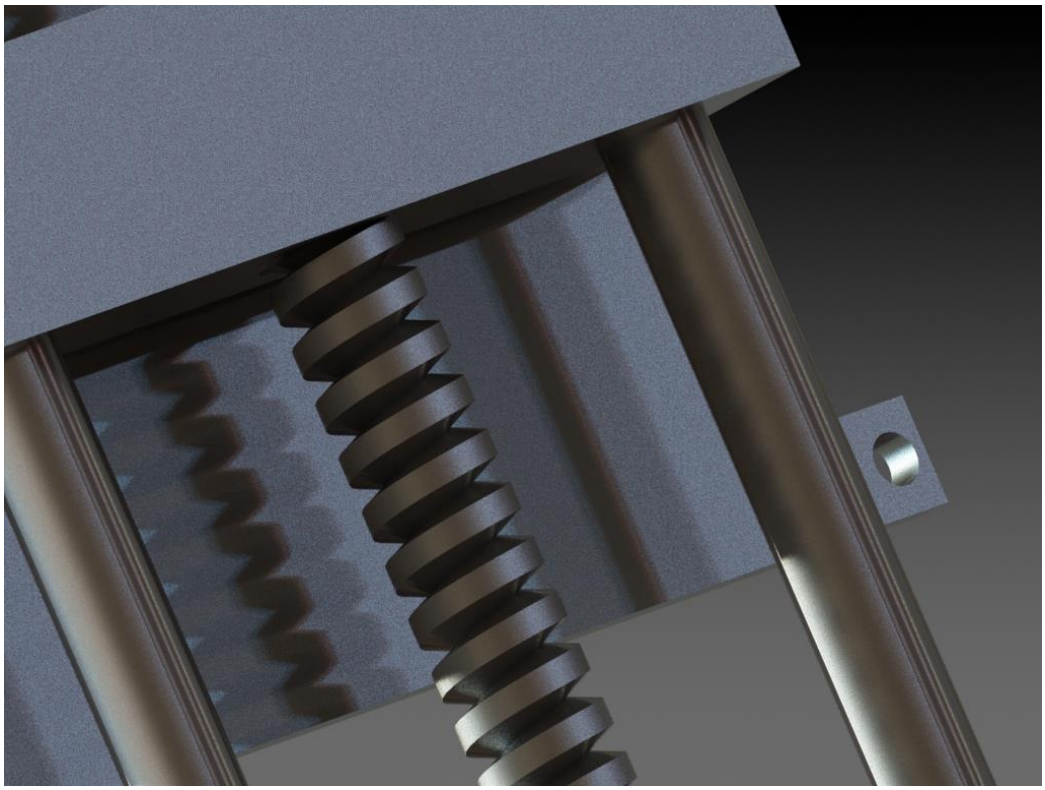

Figure 4. 11: CAD assembly of lead screw (back)

CHAPTER 5

EXPERIMENTATION

5.1. INTRODUCTION

Investigators performed experiments in all field to find out about a particular system or process. A scientific approach towards planning of the experiment is very necessary for efficiently conducting the experiment. By the statistical design of experiments the process of planning the experiment is carried out, so that appropriate data will be collected and analyzed by statistical methods resulting in unbiased valid and objective conclusions. Thus, experimental problem has two aspects:

- Design Of Experiments (DOE)
- Statistical analysis of the data

It is highly essential to design an experiment to determine the effects of variable and welding parameters on the various welding responses on a sound basis rather than a commonly employed trial and error basis in conjunction with a small number of repeat experiments for confirmation of results. Apart from the trial and error method of investigation the following techniques are commonly employed by researches:

- General quantitative approach
- Theoretical approach
- Qualitative approach
- Qualitative cum dimensional analysis method

5.1.1. General Quantitative approach

This method is commonly used for the design of experiment for research to predict the effect of input parameter on the output parameter of the experiment. Regression equation are established on the basis of the factorial design. The correlation co-efficient is a number between +1 and -1. Which are the two levels in an experimental design. Which has an intermediate value of zero. Which indicates the absence of correlation. But it does not mean that variations are also independent. The limiting value of correlation co-efficient indicates perfect positive or negative correlation. The F-

ratio is measure of scatter of the observed values about a predicted curve. The F value lies between zero and infinity. It is evident from the comparison of various research techniques that the general quantitative approach is based on a more sound logic than any other approach for the generalization of research data. Thus it was decided to make the approach, the basis of designing the experiments. There are various techniques available from the statistical theory of experimental design, which are well suited to engineering investigations. One such technique is a two level factorial design for studying the effects of parameters of responses, and this is one, which is selected for experiments. The advantages of "design of experiments" are as follows:

- Numbers of trials is significantly reduced
- Important decision variables which control and improve the performance of the product or the process can be identified
- Optimal setting of the parameters can be achieved
- Qualitative estimation of parameters can be made
- Experimental error can be estimated
- Inference regarding the effect of parameters on the characteristics of the process can be made[28].

5.2. FULL FACTORIAL DESIGN METHOD AND ANALYSIS

Factorial design is a standard statistical tool to investigate the effects of number of parameters on the response or output parameter. The most important advantage of this design is that the numbers of parameters are simultaneously studies for a more complete insight into the combined effects of the parameters on the response. In addition to that the interaction between two or more parameters can also be evaluated which is not possible with the conventional approach. Since in that approach all parameters, other than one investigated are held constant. In statistics, fractional factorial designs are experimental designs consisting of a carefully chosen subset (fraction) of the experimental runs of a full factorial design. The subset is chosen so as to exploit the effects principle to expose information about the most important features of the problem studied, while using a fraction of the effort of a full factorial design in terms of experimental runs and resources. A full factorial experiment is an experiment whose design consists of two or more factors, each with values or "levels", and whose experimental units take on all possible combinations of these levels across all such factors. A full factorial design may also be called a fully crossed design.

Such an experiment allows the investigator to study the effect of each factor on the response variable, as well as the effects of interactions between factors on the response variable. For the vast majority of factorial experiments, each factor has only two levels.

If the number of combinations in a full factorial design is too high to be logistically feasible, a fractional factorial design may be done, in which some of the possible combinations (usually at least half) are omitted [29].

Many experiment involve the study of the effects of two or more factors. In general, factorial design are most efficient for this type of experiment. By a factorial design, we mean that in each complete trial or replication of the experimentally possible combinations of the levels of the factors are investigated. For example, if there are *a* levels of factor A and *b* levels of factor B, each replicate contains all *ab* treatment combinations. When factors are arranged in a factorial design, they are often said to be crossed.

The effect of a factor is defined to be the change in response produced by a change in the level of the factor. This is frequently called a main effect because it refers to the primary factors of interest in the experiment. For example, consider the simple experiment in figure 5.1. This is a two factor factorial experiment with both design factor at two levels. We have called these levels "low" and "high" and denoted them "-" and "=" respectively. The main effect of factor A in this two level design can be thought of as the difference between the average response at the low levels of A and the average response at the high levels of A. Numerically, this is

$$A = \frac{40 + 52}{2} - \frac{20 + 30}{2} + 21$$

That is increasing factor A from the low level to the high level causes an average response increase of 21 units. Similarly, the main effect of B is

$$B = \frac{30 + 52}{2} - \frac{20 + 40}{2} + 11$$

If the factor appear at more than two levels, the above procedure must be modified because there are other ways to define the effect of a factor. This point is discussed more completely later.

In some experiment, we may find that the difference in response between the levels of one factor is not the same at all levels of the other factors. When this occurs, there is an interaction between the factors. For example, consider the two factor factorial experiment shown in Figure 5.2.

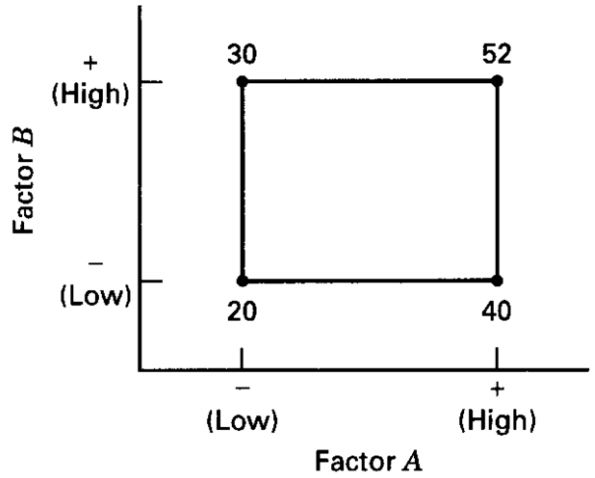

Figure 5. 1: A two factor factorial experiment, with the response (y) shown at the corners

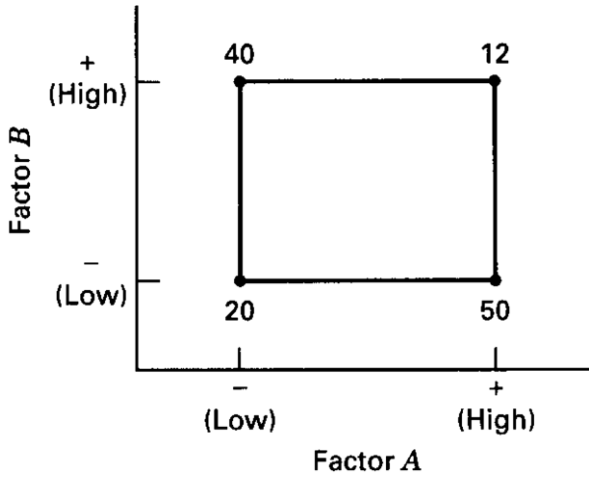

Figure 5. 2: A two factor factorial experiment with interaction

At the low level of factor A (or A^-), the A effect is and at the high level of factor B (or B^-), the A effect is

$$A= 50 – 20 = 30$$

$$A = 12 – 40 = - 28$$

Because the effect of A depends on the level chosen for factor B, we see that there is interaction between A and B. The magnitude of the interaction effect is the average difference in these two A effect, of AB = (-28 -30)/2 = -29. Clearly, the interaction is large in this experiment.

These instead may be illustrated graphically. Figure plots the response data in figure against factor A for both levels of factor B. Note that the B^- and B^+ lines are approximately parallel, indicating a lack of interaction between factor A and B. Similarly, figure plot the response data in figure. Here we see that the B^- and B^+ lines are not parallel. This indicates an interaction between factors A and B. graphs such as these are frequently very useful in interpretation significant interactions and in reporting results to non-statistically trained personnel. However, they should not be utilized as the sole technique of data analysis because their interpretation is subjective and their appearance if often misleading [29].

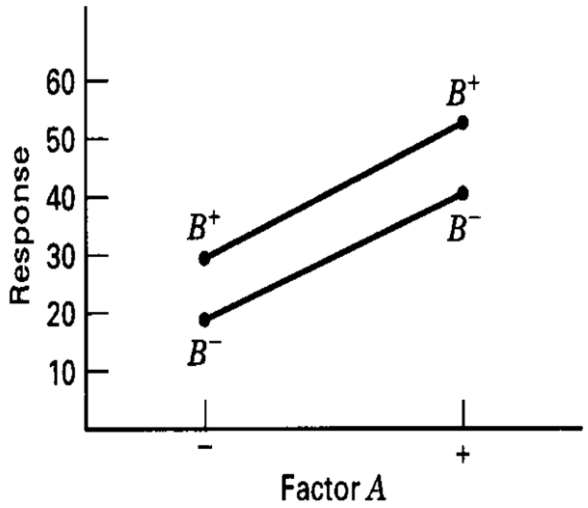

Figure 5. 3: A factorial experiment without interaction

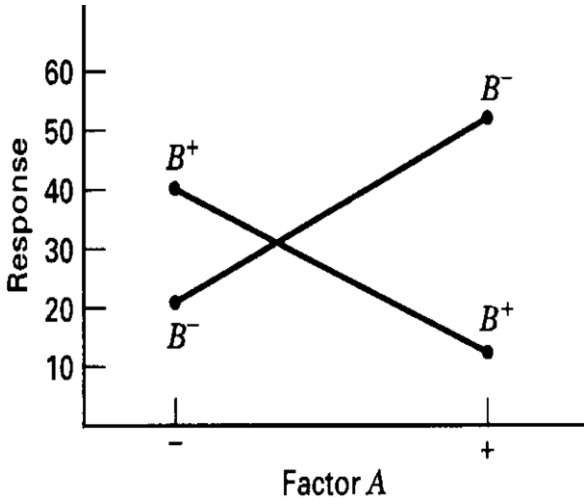

Figure 5. 4: A factorial experiment with interaction

There is another way to illustrate the concept of interaction. Suppose that both off our design factr are quantitative. Then a regression model representation of the two-factor factorial experiment could be written as

$$y=\beta o+\beta 1x1+\beta 2x2+\beta 12x1x2+\epsilon$$

where y is the response, the β's are parameters whose values are to be determined, x1 is a variable that represents factor A,x2 is a variable that represents factor B, and ϵ is a random error term. The variables x1 and x2 are defined on a coded scale from -1 to +1 (the low and high levels of A and B), and x1x2 represents the interaction between x1 and x2[29].

5.3. MERITS AND DEMERITS OF FACTORIAL DESIGN

Factorial designs are extremely useful to psychologists and field scientists as a preliminary study, allowing them to judge whether there is a link between variables, whilst reducing the possibility of experimental error and confounding variables.

The factorial design, as well as simplifying the process and making research cheaper, allows many levels of analysis. As well as highlighting the relationships between variables, it also allows the effects of manipulating a single variable to be isolated and analyzed singly.

The main disadvantage is the difficulty of experimenting with more than two factors, or many levels. A factorial design has to be planned meticulously, as an error in one of the levels, or in the general operationalization, will jeopardize a great amount of work.

Other than these slight detractions, a factorial design is a mainstay of many scientific disciplines, delivering great results in the field [30].

5.4. DESIGN OF EXPERIMENT

The main aim of this project was to find the effect of input process variable on the mechanical properties of GTAW of copper and stainless steel and develop mathematical models to describe the relationship between the input and output variables. Metallurgical analysis was also done to co-relate the effect of input parameters on the tensile strength, hardness and microstructure of the weld specimen. To achieve the above mentioned objective, following are the sequence of steps which were carried out:

5.5. STEPS OF PLAN OF INVESTIGATION

The research work was planned to be carried out in following steps:

1) Identification of important process control variables.
2) Deciding the working range of the process control variables viz. Welding Current (C), Gas flow Rate (G), Off Set (O), Speed (S)
3) Develop the design matrix.
4) Conduction of the experimentation as per the developed design matrix.
5) Record the responses
   (viz. Ultimate Tensile Strength)
6) Develop the mathematical models.
7) Checking the adequacy of the models.
8) Finding the significance of co-efficient.
9) Developing the final proposed models.
10) Plotting of graphs and drawing conclusions.
11) Discussion of the results

5.5.1. Identification of important process control variables

On the basis of weldability of metal four independently controllable process parameters were identified namely:

- Welding Current (C)

- Gas flow rate (G)
- Offset (O)
- Speed (S)

The response parameter chosen for this study was Ultimate Tensile Strength

5.5.2. Deciding the working range of process control variables

To decide the working range of process control variables. Trial runs were conducted by varying one of the process parameters at a time while keeping the rest of them at constant value. Process control variables include Welding current, Gas Flow Rate, Offset, Speed. The range obtained is given below in the table:

Table 5. 1: Working range of process variables

S.No	Parameters	Unit	Notation
1	Welding current	Ampere	C
2	Gas flow rate	L/Min	G
3	Offset	mm	O
4	speed	mm/Min	S

On the basis of working range of process variables, upper and lower limits are coded as +1 and -1 respectively. The coded values for intermediate values were then calculated from the relationship:

$$X_i = \frac{2[2X - (X_{max} + X_{min})]}{(X_{max} - X_{min})}$$

- Where, Xi is the required coded value of a variable X,
- when X is any value of the variable from Xmin to Xmax;
- Xmax and Xmin are the maximum and minimum levels of the variables

The selected process parameters and their upper and lower limits together with notations and units are given in Table

Table 5. 2: Upper and lower limit of welding parameters

S. no	Parameters	Units	Notation	-1	+1
1.	Welding current	Ampere	C	140	145
2.	Gas flow rate	L/Min	G	5	10
3.	Offset	mm	O	1	2.4
4.	Speed	mm/Min	S	2.74	2.93

5.5.3. Developing the Design Matrix

Factorial design can be represented in the form of design matrix where column and row corresponds to levels of factors and different experimental runs. The sign of input parameters of design matrix were selected in such a way that they have certain necessary optimal properties, which are as given below**:**

Symmetry related to the centre of the experiment

The algebraic sum of the elements of the column vector of each parameter should be equal to zero.

$$\sum_{i=1}^{N} X_{ij} = 0$$

Where,

i = number of factors

N = number of trials, j=1, 2.....k

Table Design Matrix

5.5.4. Conducting the experiments as per the design matrix

For conducting the experiments as per the design matrix, the welding laboratory of Delhi Technological University was used with given welding set-up. For carrying out the research work, test specimens were prepared from 1.5 mm thickness Copper and 304 stainless steel. Dimensions of each late were 75x50x1.5 mm. thirty two sets of plates were welded as per the design matrix by selecting trials at random. Figure shows four sets of welded specimen

Table 5. 3: Design matrix with input parameters

Weld No.	Input parameters				
	Trial No.	C	G	O	S
1	1	-	-	-	-
2	2	+	-	-	-
3	9	-	+	-	-
4	3	+	+	-	-
5.	10	-	-	+	-
6.	4	+	-	+	-
7	11	-	+	+	-
8	5	+	+	+	-
9	12	-	-	-	+
10	6	+	-	-	+
11	13	-	+	-	+
12	7	+	+	-	+
13	14	-	-	+	+
14	8	+	-	+	+
15	15	-	+	+	+
16	16	+	+	+	+

5.5.5. Material

For carrying out the research work, test specimens were prepared from 1.5mm thick copper plate. Dimension of each plate was 75X50X1.5 mm. Composition of the metal is identified by spectro analysis using Hilger Polyvac 2000 optical Emission Spectrometer. Optical emission spectrometry involves applying electrical energy in the form of spark generated between an electrode and a metal sample, whereby the vaporized atom are bought to a high energy state within a so called "discharged plasma". These excited atoms and ions in the discharge plasma create a unique emission spectrum specific to each element.

1. **Spectro Analysis of copper and stainless steel**

   In the Optical Emission Spectroscopy technique, atoms in a sample are excited by energy that comes from a spark formed between sample and electrode. The energy of the spark causes the electrons in the sample to emit light which is converted into a spectral pattern. By measuring the intensity of the peak in this spectrum, OES analysers can produce qualitative and quantitative metal analysis of the material composition with uncompromising accuracy.

2. **Microscopic Examination of copper and stainless steel**

   The primary objective of metallography examination is to reveal the constitutes and structure of metal and their alloys by means of a light optical or scanning electron microscope. In special cases, the objective of the examination may require the development of less detail than in other cases but, under nearly all conditions, the proper seletion and preparation of the specimen is of major importance. Radical 40 XS-800x Metallurgical Microscope with 5MP camera is used for examination [31].

Table 5. 4: Material composition stainless steel

ELEMENT	PERCENTAGE
Iron	71.47
Carbon	0.048
Silicon	0.185
Manganese	1.06
Sulphur	<0.005
Phosphorus	0.0220
Nickel	8.05
Chromium	18.48
Molybdenum	0.227
Vanadium	0.098
Titanium	0.098
Copper	0.299
Niobium	0.041
Aluminium	<0.01

Table 5. 5: Material composition of copper

ELEMENT	PERCENTAGE
Copper	99.84
Tin	0.0460
Lead	0.0050
Phosphorus	0.0220
Cobalt	0.0010
Nickel	0.0570
Silver	0.0180
Zinc	0.0012

Eight sets of plate were welded as per the design matrix by selecting trials at random and welding was carried out. Figure 5.5 shows few samples in welded condition.

Figure 5. 5: Welded samples

5.4.6. Recording the Responses

1. Hardness Test

Micro Hardness tests are used in mechanical engineering to determine the hardness of a material to deformation. Several such tests exist, wherein the examined material is indented until an impression is formed; these tests can be performed on a macroscopic or microscopic scale. When testing metals, indentation hardness correlates linearly with tensile strength. This relation permits economically important nondestructive testing of bulk metal deliveries with lightweight, even portable equipment, such as hand-held Rockwell hardness testers.

Hardness measurements quantify the resistance of a material to plastic deformation. Indentation hardness tests compose the majority of processes used to determine material hardness, and can be divided into two classes: microindentation and macroindentation tests. Microindentation tests typically have forces less than 2 N (0.45 lbf). Hardness, however, cannot be considered to be a fundamental material property. Instead, it represents an arbitrary quantity used to provide a relative idea of material properties.

Figure 5. 6: Hardness testing machine

Figure 5. 7: Micro hardness tester

Another effect the load has on the indentation is the piling-up or sinking-in of the surrounding material. If the metal is work hardened it has a tendency to pile up and form a "crater". If the metal is annealed it will sink in around the indentation. Both of these effects add to the error of the hardness measurement.

The equation based definition of hardness is the pressure applied over the contact area between the indenter and the material being tested. As a result hardness values are typically reported in units of pressure, although this is only a "true" pressure if the indenter and surface interface is perfectly flat.

The term "microhardness" has been widely employed in the literature to describe the hardness testing of materials with low applied loads. A more precise term is "microindentation hardness testing." In microindentation hardness testing, a diamond indenter of specific geometry is impressed into the surface of the test specimen using a known applied force (commonly called a

"load" or "test load") of 1 to 1000 gf. Microindentation tests typically have forces of 2 N (roughly 200 gf) and produce indentations of about 50 μm. Due to their specificity, microhardness testing can be used to observe changes in hardness on the microscopic scale. Unfortunately, it is difficult to standardize microhardness measurements; it has been found that the microhardness of almost any material is higher than its macrohardness. Additionally, microhardness values vary with load and work-hardening effects of materials.The two most commonly used micro hardness tests are tests that also can be applied with heavier loads as macro indentation tests:

- Vickers hardness test (HV)
- Knoop hardness test (HK)

In micro indentation testing, the hardness number is based on measurements made of the indent formed in the surface of the test specimen. The hardness number is based on the surface area of the indent itself divided by the applied force, giving hardness units in kgf/mm². Micro indentation hardness testing can be done using Vickers as well as Knoop indenters. For the Vickers test, both the diagonals are measured and the average value is used to compute the Vickers pyramid number. In the Knoop test, only the longer diagonal is measured, and the Knoop hardness is calculated based on the projected area of the indent divided by the applied force, also giving test units in kgf/mm².

The Vickers micro indentation test is carried out in a similar manner to the Vickers macro indentation tests, using the same pyramid. The Knoop test uses an elongated pyramid to indent material samples. This elongated pyramid creates a shallow impression, which is beneficial for measuring the hardness of brittle materials or thin components. Both the Knoop and Vickers indenters require prepolishing of the surface to achieve accurate results

There is some disagreement in the literature regarding the load range applicable to microhardness testing. ASTM Specification E384, for example, states that the load range for microhardness testing is 1 to 1000 gf. For loads of 1 kgf and below, the Vickers hardness (HV) is calculated with an equation, wherein load (L) is in grams force and the mean of two diagonals (d) is in millimeters:

$$HV = 0.0018544 \times \frac{L}{d^2}$$

For any given load, the hardness increases rapidly at low diagonal lengths, with the effect becoming more pronounced as the load decreases. Thus at low loads, small measurement errors will produce large hardness deviations. Thus one should always use the highest possible load in

any test. Also, in the vertical portion of the curves, small measurement errors will produce large hardness deviations [32].

2. Weld Metallurgy

Stainless Steel is a generic term covering a large group of iron based, chromium containing alloys. The term "stainless" implies a resistance to staining or rusting in air, which requires a minimum of 10.5% chromium to form a thin, protective chromium enriched oxide layer on the surface of the steel. Without the addition of chromium, iron based alloys or steels will corrode in moist air, forming the familiar red rust. Figure shows the equilibrium diagram for combinations of carbon in a solid solution of iron. The diagram shows iron and carbons combined to form Fe-Fe_3C at the 6.67%C end of the diagram. The left side of the diagram is pure Iron combined with carbon, resulting in steel alloys. Three significant regions can be made relative to the steel portion of the diagram. They are the eutectoid E, the hypo eutectoid A, and the hypereutectoid B. The right side of the pure iron line is carbon in combination with various forms of iron called alpha iron (ferrite), gamma iron (austenite), and delta iron. The black dots mark clickable sections of the diagram. Allotropic changes take place when there is a change in crystal lattice structure. From 1539º-1400ºC the delta iron has a body-centered cubic lattice structure. At 1400ºC, the lattice changes from a body-centered cubic to a face-centered cubic lattice type. At 760ºC, the curve shows a plateau but this does not signify an allotropic change. It is called the Curie temperature, where the metal changes its magnetic properties [33][34][35].

Two very important phase changes take place at 0.83%C and at 4.3% C. At 0.83%C, the transformation is eutectoid, called pearlite.

Eutectic: A eutectic or eutectic mixture is a mixture of two or more phases at a composition that has the lowest melting point, and where the phases simultaneously crystallize from molten solution at this temperature. The proper ratios of phases to obtain a eutectic are identified by the eutectic point on a phase diagram.

Eutectoid: When the solution above the transformation point is solid, rather than liquid, an analogous eutectoid transformation can occur. For instance, in the iron-carbon system, the

austenite phase can undergo a eutectoid transformation to produce ferrite and cementite (iron carbide), often in lamellar structures such as pearlite and bainite.

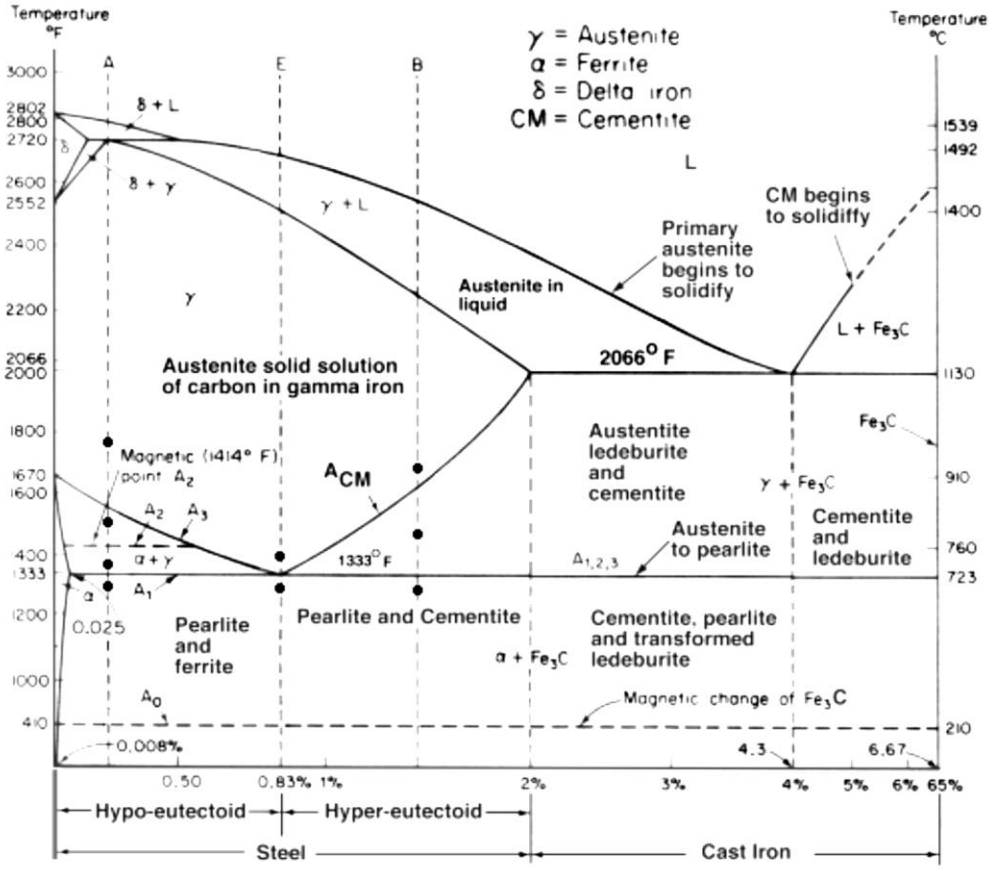

Figure 5. 8: Iron Carbon Diagram (Courtesy of www.google.com)

Since low-alloy steels are basically of the oil- or air hardening types it follows that martensite is very likely to form in the heat affected zone during subsequent cooling giving rise to 'cold cracking'. Where possible the whole weldment is preheated to between Ms and Mt temps and held there for up to thirty minutes after welding is complete so that isothermal transformation of austenite to bainite will occur and frustrate the formation of martensite which would other wise take place during cooling.

The problems associated with welding stainless steels depend upon whether the steels are of the ferritic or austenitic types. Ferritic high chromium steels suffer from grain growth in the heat affected zone and also the formation of martensite if the steel contains sufficient carbon and is permitted to cool at a rate which will give rise to air-hardening.

a) Weld pool solidification

Most knowledge of weld pool solidification is derived from the extrapolation of the knowledge of freezing of castings, ingots, and single crystals at lower thermal gradients and slower growth rates. Therefore, parameters important in determining microstructures in casting, such as growth rate (R), temperature gradient (G), undercooling (δT), and alloy composition determine the development of microstructures in welds as well. However, microstructure development in the weld zone is more complicated because of physical processes that occur due to the interaction of the heat source with the metal during welding, including re-melting, heat and fluid flow, vaporization, dissolution of gasses, solidification, subsequent solid-state transformation, stresses, and distortion. These processes and their interactions profoundly affect weld pool solidification and microstructure. During welding, where the molten pool is moved through the material, the growth rate and temperature gradient vary considerably across the weld pool. Along the fusion line the growth rate is low while the temperature gradient is steepest. As the weld centerline is approached, the growth rate increases while the temperature gradient decreases. Consequently, the microstructure that develops varies noticeably from the edge to the centre line of the weld. In welds, weld pool solidification often occurs spontaneously by epitaxial growth on the partially melted grains. Since solidification of the weld metal proceeds spontaneously by epitaxial growth of the partially melted grains in the base metal, the weld zone grain structure is mainly determined by the base metal grain structure and the welding conditions. Crystallographic effects will influence grain growth by favouring growth along particular crystallographic directions, namely the easy growth directions. Conditions for growth are optimum when one of the easy growth directions coincides with the heat-flow direction. Thus, among the randomly oriented grains in a polycrystalline specimen, those grains that have one of their easy growth crystallographic axes closely aligned with heat-flow direction will grow at the expense of their neighboring less favorably oriented grains. This is called competitive growth. Without additional nucleation, this will promote a columnar grain structure. Low values of $G/(R)^{1/2}$ indicate as increased tendency to constitutional super cooling thus favouring the dendritic mode of solidification. On the other hand steep temperature gradients in the liquid and slow growth rates favors cellular growth.

b) Welding zones

Weld metal zone is formed as the weld metal solidifies from the molten state. This is a mixture of parent metal, electrode, filler metal; the ratio depending upon the welding process used, the type of joint plate thickness. Weld metal zone is a cast metal of particular composition of mixture that has cooled; its microstructure reflects the cooling rate in the weld. Depending upon the chemical composition a martensitic structure in the weld indicates a very high cooling rate; fine pearlite and coarse pearlite shows comparatively slower cooling rates. From the molten weld pool the first metal solidifies epitaxially upon the solid grains of the un-melted base metal. Depending upon the composition and solidification rates the weld solidifies in a cellular or dendritic growth mode. Both modes cause segregation of alloying elements and consequently the weld metal is less homogeneous on the micro level than the base metal and therefore cannot be expected to have the same properties as wrought parent metal unless the filler metal in the as deposited condition has same properties as that of parent metal.

c) Heat Affected Zone:

It consists of parent metal that did not melt but was heated to high enough temperature for a sufficient period of time that grain growth occurred and mechanical as well as microstructural properties have been altered by the heat of welding. The HAZ is subjected to complex thermal cycle in which all temperatures from the melting range of the steel down to comparatively much lower temperatures are involved. HAZ usually consists of a variety of microstructures. These structures may range from very narrow regions of hard martensite to coarse pearlite. This renders HAZ the weakest area in weld. Except where there are obvious defects in the weld deposit, most welding failures originate in the HAZ. In SAW the HAZ consists of 3sub zones

I. Grain growth region: It is immediately adjacent to the weld metal zone. In this zone the parent metal has been heated well above the upper critical temperature, this resulted in grain growth or coarsening of the structure. The maximum grain size and extent of this region increases as the cooling rate decreases.
II. Grain refined region: The refined zone indicates that in this region the parent metal has been heated to just above upper critical temperature where grain refinement is complete and finest grain structure exists. Complete recrystallization has taken place in this zone

III. Transition zone: Temperature exists between upper and lower recrystallization temperature where partial allotropic recrystallization takes place.

3. Tensile Test

Tensile test, also known as tension test, is a fundamental material science test in which a sample is subjected to a controlled tension until failure. The result from the test are commonly used to select a material for an application, for quality control, and to predict how a material will react under other types of forces. Properties that are directly measured via a tensile test are ultimate tensile strength, maximum elongation and reduction in area. From these measurements the following properties can also be determined: Young's modulus, Poisson's ratio, yield strength, and strain-hardening characteristics. Refer to Figure 5.9 and Figure 5.10.

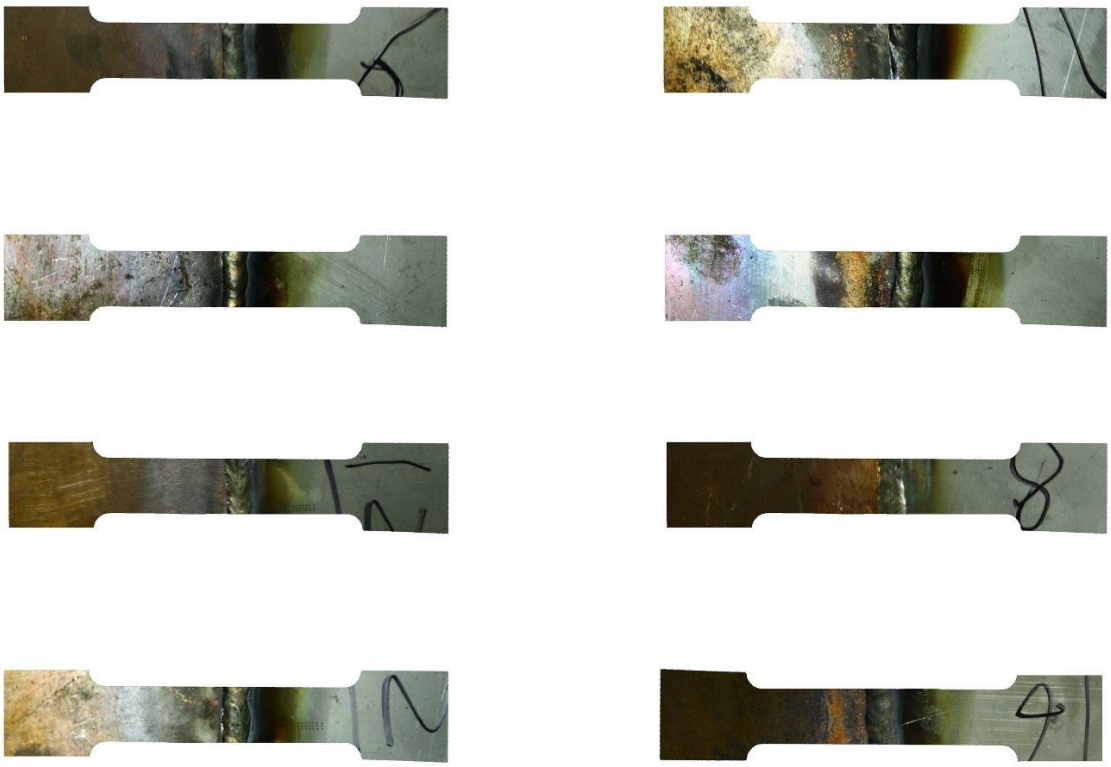

Figure 5. 9: Specimens for tensile test

Figure 5. 10: Specimen after tensile test

The response Ultimate Tensile Strength is in the tables given below :

Table 5. 6: Recording of UTS

Weld No.	Trial No.	Input parameters				Responses	
		C	G	O	S	UTS 1	UTS 2
1	1	-	-	-	-	209	191
2	2	+	-	-	-	189	170
3	9	-	+	-	-	182	194
4	3	+	+	-	-	180	190
5	10	-	-	+	-	191	211
6	4	+	-	+	-	196	208
7	11	-	+	+	-	198	195
8	5	+	+	+	-	193	190
9	12	-	-	-	+	188	195
10	6	+	-	-	+	174	192
11	13	-	+	-	+	180	180
12	7	+	+	-	+	170	173
13	14	-	-	+	+	185	197
14	8	+	-	+	+	180	188
15	15	-	+	+	+	192	185
16	16	+	+	+	+	182	180

CHAPTER 6

DEVELOPMENT OF MATHEMATICAL MODEL

Mathematical models can be proposed as the basic for a control system or the GTAW process to predict particular mechanical property and to establish the inter relationship between weld process parameters to weld mechanical property. These mathematical models can be fed into computer to predict the mathematical property for a particular combination of input parameters. The experimental data were used to develop multi linear regression models, and analysis of the models were carried out through ANOVA . Minitab 17.0 was used for this purpose.

6.1. FORMULATION OF MATHEMATICAL MODEL:

The response function can be expressed as: Y = Ϯ(C,G,O,S)

Where, Y= response

C = Current

G = Gas flow rate

O = Offset

S = Speed

A linear regression model with four predictor variable can be expressed with the following equation:

$$Y = b_0 + b_1C + b_2G + b_3O + b_4S + b_{12}CG + b_{13}CO + b_{14}CS + b_{23}GO + b_{24}GS + b_{34}OS + b_{123}CGO + b_{124}CGS + b_{134}COS + b_{234}GOS + b_{1234}CGOS$$

Where b_0 is constant and $b_0, b_1, b_2, b_3, b_4, b_{12}, b_{13}, b_{14}, b_{23}, b_{24}, b_{34}, b_{123}, b_{124}, b_{134}, b_{234}, b_{1234}$ are co-efficients of model b_0 , the Y-intercept, can be interpreted as the value to predict for Y if C=G=O=S=0

Since C is a continuous variable, b_1 represents the difference in the predicted value of Y for each one-unit difference in C, if other independent variable remains constant. This means that if N is differed by one unit G, O and S did not differ, Y will differ by b_1 units, on average.

6.2. EVALUATION OF THE CO-EFFICIENT OF MODEL

The value of the co efficient of the response function were calculated using regression analysis. The calculation were carried out using MINITAB 17 and the values listed in table 6.1.

Table 6. 1: Estimated value of the coefficients of the model

S.NO	Co-efficient	Tensile Strength
1	b_0	200.00
2	b_1	-20.50
3	b_2	-12.0
4	b_3	1.00
5	b_4	-8.50
6	b_{12}	17.50
7	b_{13}	21.50
8	b_{14}	12.00
9	b_{23}	7.50
10	b_{24}	0.50
11	b_{34}	-1.50
12	b_{123}	-23.50
13	b_{124}	-17.50
14	b_{134}	1.50
15	b_{234}	-20.00
16	b_{1234}	23.00

The responses (mechanical properties) is expressed as a linear function of the input process parameters as follows:

Tensile Strength (TS) = $b_0 + b_1C + b_2G + b_3O + b_4S + b_{12}CG + b_{13}CO + b_{14}CS + b_{23}GO + b_{24}GS + b_{34}OS + b_{123}CGO + b_{124}CGS + b_{134}COS + b_{234}GOS + b_{1234}CGOS$

Tensile Strength (TS) = $200 - 20.50 \times C - 12 \times G + 1 \times O - 8.50 \times S + 17.50 \times CG + 21.50 \times CO + 12 \times CS + 7.50 \times GO + 0.50 \times GS - 1.50 \times OS - 23.50 \times CGO - 17.50 \times CGS + 1.50 \times COS - 20 \times GOS + 23 \times CGOS$

6.3. CHECKING ADEQUACY OF THE MODEL

Analysis of variance (ANOVA) is a procedure for assigning sample variance to different source and decide whether the variation arises within or among different population groups. Sample are described in terms of variation around group means and Variation of groups means around an overall mean. If variation within groups are small relative to variation between groups, a different in group means may be inferred. Hypothesis tests are used to quantify decisions.

The analysis of variance (ANOVA) was used to check the adequacy of the developed models. As per this technique:

a) The F-ratio of the developed model is calculated and is compared with the standard tabulated value of F-ratio for a specific level of confidence.
b) If calculated value of F-ratio does not exceed the tabulated value, then with the corresponding confidence probability the model may be considered adequate. For analysis, a confidence interval of 95% is taken [36].

6.3.1. ANOVA : Tensile Strength

Calculated value of F-ratio for the selected model is 2.240. Tabulated value corresponding to the probability confidence (95%) is 4.49 for degree of freedom 1, 16 numerator and denominator. As calculated value of F-ratio does not exceed tabulated value, the model can be considered adequate. For 95% confidence level the P-value should be less than 0.05. If the P-value lies below 0.05 then it can be said that the values are statistically significant.

Table 6. 2: ANOVA or tensile strength

SOURCE	DF	SUM OF SQUARES	MEAN SQUARE	F-VALUE	P-VALUE	Statistically significant
MODEL	15	2240.5	149.367	2.240	0.060	
C	1	435.125	435.125	6.525	0.021	YES
G	1	312.5	312.5	4.686	0.046	YES
O	1	406.125	406.125	6.090	0.025	YES
S	1	666.125	666.125	9.989	0.006	YES
C×G	1	15.125	15.125	0.227	0.640	
C×O	1	60.5	60.5	0.907	0.355	
C×S	1	2	2	0.030	0.865	
G×O	1	10.125	10.125	0.152	0.702	
G×S	1	6.125	6.125	0.092	0.766	
O×S	1	50	50	0.750	0.399	
C×G×O	1	2	2	1.080	0.314	
C×G×S	1	18	18	0.270	0.611	
C×O×S	1	36.125	36.125	0.542	0.472	
G×O×S	1	84.5	84.5	1.267	0.277	
C×G×O×S	1	66.125	66.125	0.992	0.334	
ERROR	16	1067	66.688			
TOTAL	31	3307.5				

6.3.2. Prediction of responses by regression model

By substituting the input in the final proposed models, the tensile strength are predicted and tabulated as follows:

Table 6. 3: Predicted tensile strength value

WELD NO	CURRENT	GAS	OFF SET	SPEED	Predicted Tensile Strength
1	140	5	1	2.74	200
2	145	5	1	2.74	179.5
3	140	10	1	2.74	188
4	145	10	1	2.74	185
5	140	5	2.4	2.74	201
6	145	5	2.4	2.74	202
7	140	10	2.4	2.74	196.5
8	145	10	2.4	2.74	191.5
9	140	5	1	2.93	191.5
10	145	5	1	2.93	183
11	140	10	1	2.93	180
12	145	10	1	2.93	171.5
13	140	5	2.4	2.93	191
14	145	5	2.4	2.93	184
15	140	10	2.4	2.93	188.5
16	145	10	2.4	2.93	181

6.3.3. Testing the model

The developed model were tested for the accuracy of their predictive ability. Ten test cases were selected at random from the design matrix and the experimental mechanical properties were compared to the parameters obtained from the mathematical models. The result are summarized in the table 6.4 below

Table 6. 4: Testing of mathematical mode

WELD NO	CURRENT	GAS	OFF SET	SPEED	Actual UTS	Predicted UTS	% Error
1	140	5	1	2.74	209	200	4.30
3	140	10	1	2.74	182	188	-3.29
4	145	10	1	2.74	180	185	-2.77
7	140	10	2.4	2.74	198	196.5	0.75
9	145	5	1	2.74	170	179.5	-5.58
15	140	10	2.4	2.93	192	188.5	1.82
16	145	10	2.4	2.93	182	181	0.54

CHAPTER 7

RESULTS & DISCUSSION

7.1. ULTIMATE TENSILE STRENGTH RESULT

Tensile testing also known as tension testing is a fundamental materials science test in which a sample is subjected to a controlled tension until failure. The results from the test are commonly used to select a material for an application, for quality control and to predict how a material will react under other types of forces.

Table 7. 1: Ultimate tensile strength

Sample	Ultimate Stress (Mpa)	
	A	B
1	209	191
2	189	170
3	182	194
4	180	190
5	191	211
6	196	208
7	198	195
8	193	190
9	188	195
10	174	192
11	180	180
12	170	173
13	185	197
14	180	188
15	192	185
16	182	180

7.2. MAIN EFFECT

7.2.1. Main Effect of welding parameters on UTS

UTS remains decreases from 192 to 185 when the current varies from low to high level as shown in fig 7.1. This trend may be contributed because of the metallurgical behavior of the metal. From the perusal of micrograph above it is clearly evident that the grain size is bigger in Fig 7.5 than in fig 7.6. Therefore tensile strength of the specimen that has been welded with the conditions prevailing during welding of Fig 7.5 related parameters should have been less than that of welding conditions prevailing during the welding of specimen related to fig 7.6. However the result that are obtained are contrary to the established phenomena of dissimilar joining process. This can be attributed to the test that defect are present. Consequently upon careful perusal of micrograph it is revealed that the defects in the form of porosity etc. are present and the same may have been responsible for the result that are obtained during present study. It is worthwhile to mention that the porosity may itself be the reason of arresting/ initiating/propagation of cracks and can result in erroneous behavior of joint strength value as has been experienced in the instant case.

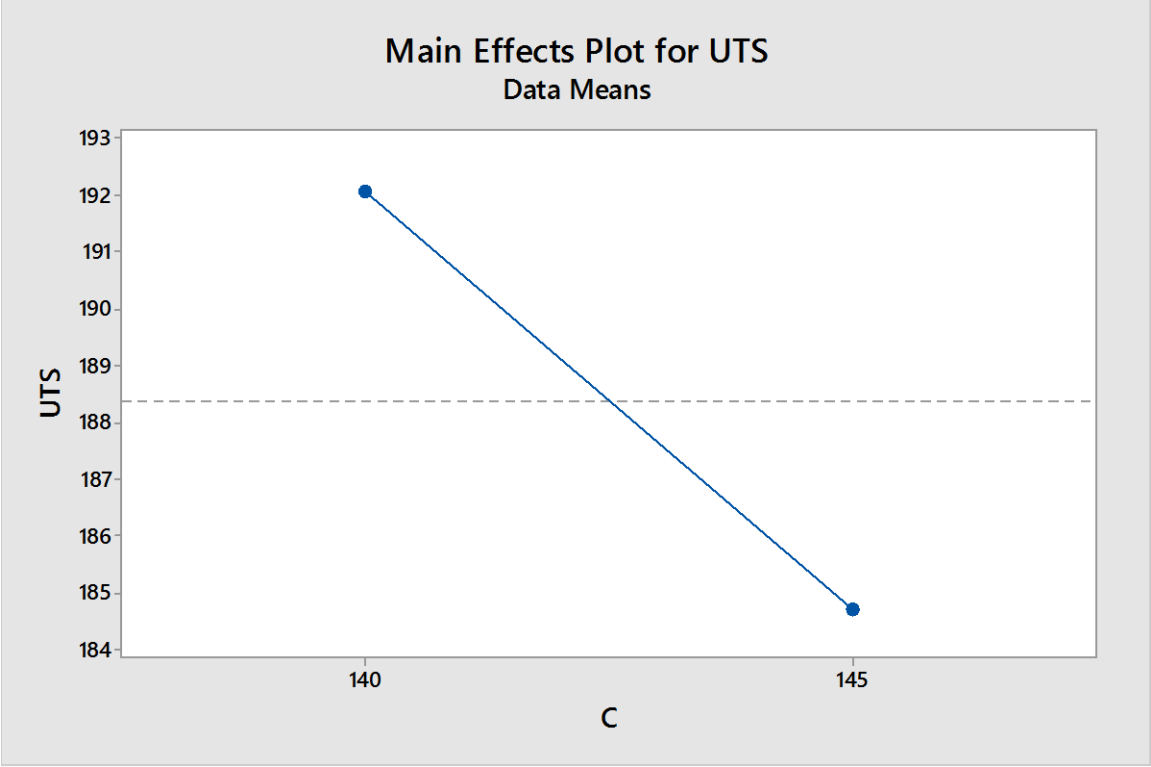

Figure 7. 1: Main effect of UTS on welding current

The tensile strength decreases 192 to 185 with increase in gas flow rate as show in Figure 7.2. The decrease in the tensile strength is because with increase in gas flow rate the depth of penetration begins to decrease linearly. Increase in gas flow rate increases the porosity formation, shielding gas traps the metal vapors in the weld pool which increases the formation of bubbles and thus decrease the tensile strength.

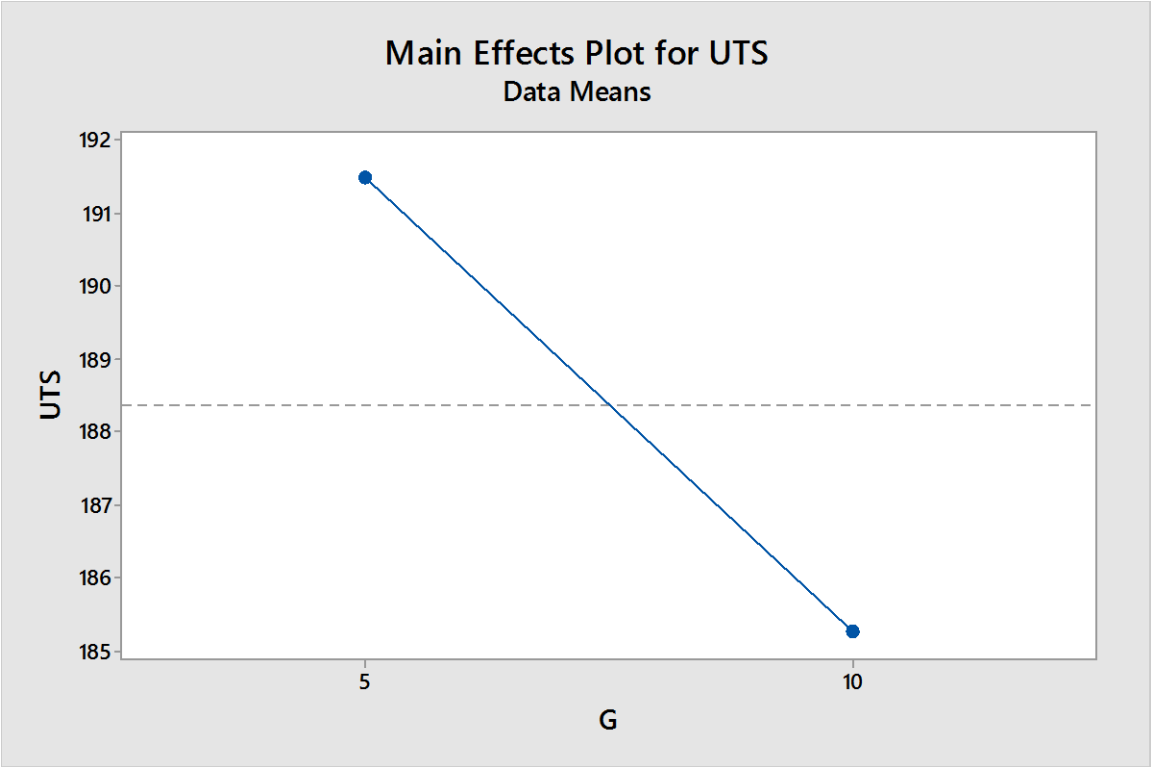

Figure 7. 2: Main effect of UTS on welding Gas

In Figure 7.3 there is an increase in tensile strength with increase in welding offset. As the offset is increased from 1mm to 2.4mm the heat generated was enough resulting in high temperature which in turn resulting in melting the stainless steel plate at the weld interface. Copper having high thermal conductivity, dissipates the heat energy so it takes log to melt where as in case of stainless steel it has low thermal conductivity. So when heat energy is applied, it results in heat concentration and melts faster.

The tensile strength decrease from 193 to 184 with increase in speed of welding from 2.74 to 2.93. This characteristic is shown because with increase in speed the heat energy decreases. With decrease in heat energy the depth of penetration decreases. Which in turn results in decrease in tensile strength.

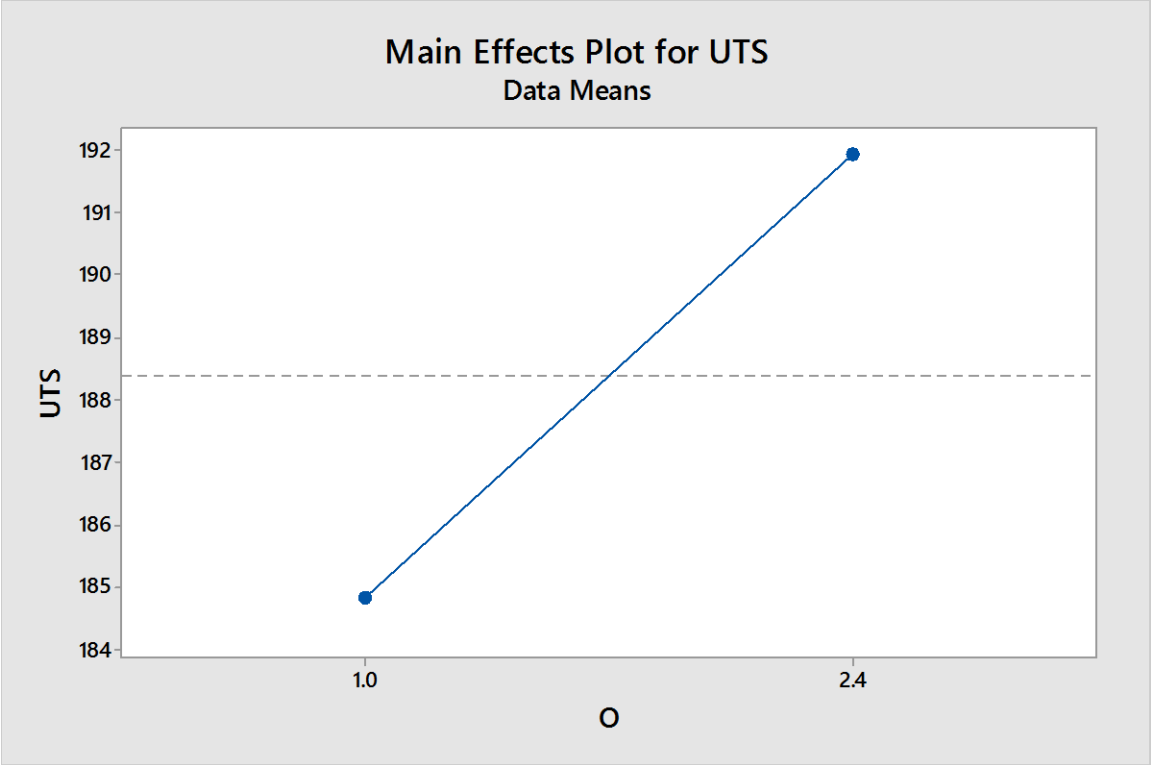

Figure 7. 3: Main effect of UTS on welding Offset

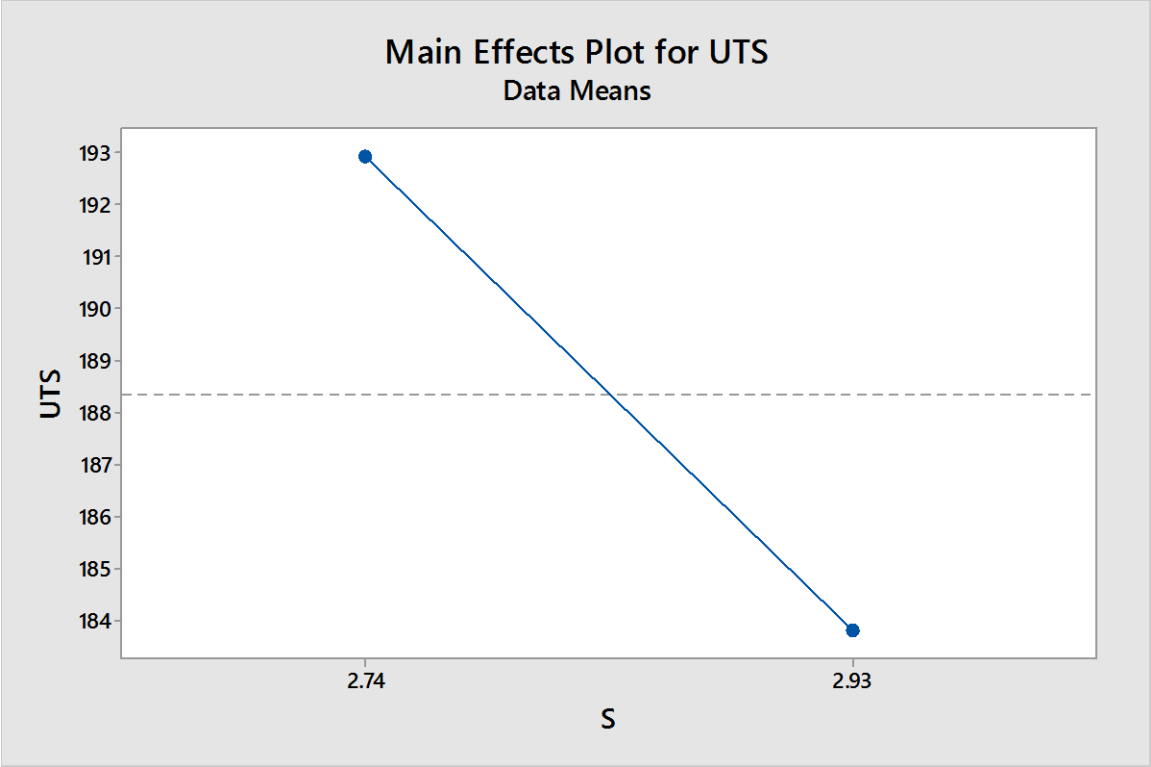

Figure 7. 4: Main effect of UTS on welding Speed

7.3. MICRO STRUCTURE

The microstructure of copper at both the heat affected zone and the weld bead was done. It was found that the microstructure at the heat affected zone (figure 7.39 & figure 7.40) of copper consist of Alpha brasses are often seen with a single phase, however this usually arises due to annealing. As the alloy cools α phase copper precipitates out first, changing the composition of the remaining melt. This may result in dendritic growth as well as the formation of other phases such as the β phase when the zinc concentration in the remaining liquid is sufficiently high. Annealing twins also appeared in the HAZ zone. These are parallel straight lines extending across many of the grains are called annealing twins. They appear after a metal has been mechanically worked at a high temperature, called annealing, and deformed. The inter-dendritic network of oxide particles was destroyed by hot rolling. After hot rolling, oxide particles changed form, and are present as stringers or aligned rows of dark particles. The oxide particles are much larger and fewer in number than in the as cast microstructure.

Figure 7. 5: Microstructure at heat affected zone, showing α-phase with annealing twins

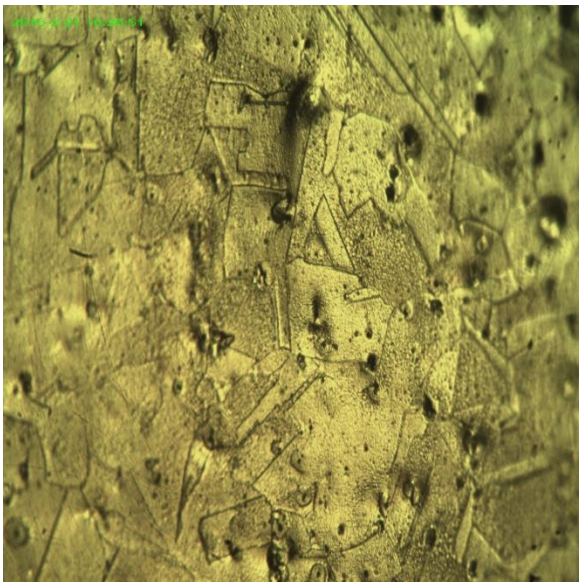

Figure 7. 6: Microstructure at heat affected zone, showing α-phase with annealing twins

Figure 7. 7: Microstructure at fusion zone showing structure consisting of dendrites in a matrix of copper

Figure 7. 8: Microstructure at fusion zone showing structure consisting of dendrites in a matrix of copper

At the Weld bead the microstructure shows that it consist of Dendrites in a matrix of copper (figure 7.41 &figure 7.42). the magnification was at 200X. This is due to the different melting temperature of the welded alloy and the steep concentration gradient arise from strong convection, which resulted in the formation of dendrites in the copper matrix

7.4. HARDNESS

Table 7. 2: Measure of hardness

S.no	Base metal	Heat affected zone	Weld bead
Sample 7	-	64-66 HV	115-118 HV
Sample 11	-	62-64 HV	154-156 HV
Sample 1	91-93 HV	-	-

It was observed that the hardness of the weld bead is more that the base metal but the hardness of the base metal at the heat affected zone was less that the base metal. This showed that the average hardness of diffusion layer (due to post heat treatment) was 154 HV, while the hardness of copper were 93 HV. It can be concluded that the ductility of diffusion layer is less than the copper.

CHAPTER 8

CONCLUSION AND SCOPE FOR FUTURE WORK

Gas tungsten arc welding of copper and stainless steel with the help of a filler material was done and which had led to a useful results.

The important conclusions from this research work are listed in section 8.1 the scope for further work that may be helpful to the manufactures, users and the researchers engaged in this technology is presented in section 8.2.

8.1. CONCLUSION

In this experiment two different metals were welded together which were copper and 304 stainless steel, with the help of gas tungsten arc welding with Brass as a filler material. The design of experiment was done by full factorial design having 4 factors and each factor had 2 levels. The following conclusions and observations were drawn from the experiment performed and analytical model predicted:

I. Ultimate tensile strength decreases with increase in current from 140 to 145A.
II. Ultimate tensile strength decreases with increase in gas flow rate from 5 to 10 L/Min.
III. Ultimate tensile strength increases with increase in offset from 1mm to 2.4mm.
IV. Ultimate tensile strength decreases with increase in speed from 2.74mm/min to 2.93mm/min.
V. The tensile strength at the heat affected zone has lower strength than copper.
VI. The micro structure at the fusion zone showed that the structure consist of dendrites in a matrix of copper. As a result the tensile strength has decreased.
VII. The micro structure at the heat affected zone of copper showed that the structure consisted of α-phase with annealing twins. As a result tensile strength of copper has been decreased.
VIII. Hardness at the fusion zone were measured and it was concluded that the hardness was more than the base metal.
IX. Hardness at the heat affected zone were measured and it was concluded that the hardness was less than the base metal.
X. The design of automated bed resulted in a constant welding speed.

8.2. SCOPE FOR FUTURE WORK

1. The effect of controlling parameters such as arc length on response variables like UTS, microstructure & hardness can also be studied.
2. Apart from the ultimate tensile strength, studies can be undertaken to analyse the effect of process parameters on yield strength and percentage elongation.
3. The welding bed can be automated with the help of micro controller to have more accurate speed.
4. Modelling of the GTAW process using Artificial Neural Network can be done and their results can be compared with existing model.
5. Optimization of process parameters can be undertaken.

REFERENCES

[1] Z Sun, R Karppi. The application of electron beam welding for the joining of dissimilar metals: An overview [J]. Journal of Materials Processing Technology, 1996, 59(3): 257−267.

[2] Ting Wang, Bing-Gang Zhang, Ji-Cai Feng. Influences of different filler metals on electron beam welding of titanium alloy to stainless steel [J]. Transactions of Nonferrous Metals Society of China, 2014, 24(1): 108−114.

[3] S G Shiri, M Nazarzadeh, M Sharifitabar, M S Afarani. Gas tungsten arc welding of CP-copper to 304 stainless steel using different filler materials [J]. Transactions of Nonferrous Metals Society of China, 2012, 22(12): 2937−2942.

[4] X J Yuan, G M Sheng, B Qin, W Z Huang, B Zhou. Impulse pressuring diffusion bonding of titanium alloy to stainless steel [J]. Materials Characterization, 2008, 59(7): 930−936.

[5] J L Yang, Y Li, F Wang, Z G Zhang, S J Li. New application of stainless steel [J]. Journal of Iron and Steel Research, International, 2006, 13: 62−66.

[6] T A Mai, A C Spowage Characterisation of dissimilar joints in laser welding of steel–kovar, copper–steel and copper–aluminium [J]. Materials Science and Engineering A, 2004, 374(1-2): 224−233.

[7] M. Velu, Sunil Bhat Experimental investigations of fracture and fatigue crack growth of copper–steel joints arc welded using nickel-base filler 67 (2015) 244–260

[8] R. Kumar, M. Balasubramanian Experimental investigation of Tie6Alе4V titanium alloy and 304L stainless steel friction welded with copper interlayer 11 (2015) 65e75

[9] Bing-Gang Zhang, Jian Zhao, Li Xiao-Peng, Ji-Cai Feng Electron beam welding of 304 stainless steel to QCr0.8 copper alloy with copper filler wire 24(2014) 4059−4066

[10] Y. Kchaou, N. Haddar, G. Hénaff, V. Pelosin, K. Elleuch Microstructural, compositional and mechanical investigation of Shielded Metal Arc Welding (SMAW) welded superaustenitic UNS N08028 (Alloy 28) stainless steel 63 (2014) 278–285

[11] M.A. García-Renteríaa, V.H. López-Morelosa, R. García-Hernándeza, L. Dzib-Pérezb,E.M. García-Ochoab, J. González-Sánchez Improvement of 70ikipedia corrosion resistance of AISI 2205 Duplex Stainless Steel joints made by gas metal arc welding under electromagnetic interaction of low intensity 321 (2014) 252–260

[12] K. Devendranath Ramkumar, G. Thiruvengatam, S.P. Sudharsan, Debidutta Mishra, N. Arivazhagan, R. Sridhar Characterization of weld strength and impact toughness in the multi-pass welding of super-duplex stainless steel UNS 32750 60 (2014) 125–135

[13] Z.H. Liu, D.Q. Zhang, S.L. Sing, C.K. Chua, L.E. Loh Interfacial characterization of SLM parts in multi-material processing: Metallurgical diffusion between 316L stainless steel and C18400 copper alloy 9 4 (2 0 1 4) 1 1 6 – 1 2 5

[14] M. Velu, Sunil Bhat Metallurgical and mechanical examinations of steel–copper joints arc welded using bronze and nickel-base superalloy filler materials [2013] (2013) 793–809

[15] Ting Wang, Binggang Zhang, Guoqing Chen, Jicai Feng High strength electron beam welded titanium stainless steel joint with V/Cu based composite filler metals [2013]

[16] R. Mendes, J.B. Ribeiro, A. Loureiro Effect of explosive characteristics on the explosive welding of stainless steel to carbon steel in cylindrical configuration [2013] 51 (2013) 182–192

[17] Shuhai Chen, Mingxin Zhang, Jihua Huang, Chengji Cui, Hua Zhang, Xingke Zhao Microstructures and mechanical property of laser butt welding of titanium alloy to stainless steel[2013] 53 (2014) 504–511

[18] I. Tomashchuk, P.Sallamand, N.Belyavina, M.Pilloz Evolution of microstructures and mechanical properties during dissimilar electron beam welding of titanium alloy to stainless steel via copper interlayer 585(2013)114–122

[19] Shuhai Chen, Jihua Huang, Jun Xia, Hua Zhang, Xingke Zhao Microstructural Characteristics of a Stainless Steel/Copper Dissimilar Joint Made by Laser Welding 10.1007/s11661-013-1693-z

[20] Gurram Mallaiah, Adepub Kumar, Ravinder Reddy Pinnintic, Madhusudhan Reddy Gankidid Effect of copper and aluminium addition on mechanical properties and corrosion 71ikipedi of AISI 430 ferritic stainless steel gas tungsten arc welds [2012] 2(3):238–249

[21] Bina Mohammad Hosein, Dehghani Farshid, Salimi Mahmoud Effect of heat treatment on bonding interface in explosive welded copper/stainless steel [2012] 45 (2013) 504–509

[22] Sajjad Gholami Shiri, Mohsen Nazarzadeh, Mahmood Sharifitabar, Mehdi Shafiee Afarani Gas tungsten arc welding of CP-copper to304 stainless steel using different filler materials 22(2012) 2937−2942

[23] Ting Wang, Bing-Gang Zhang, Guo-Qing Chen, Ji-Cai Feng, Qi Tang Electron beam welding of Ti-15-3 titanium alloy to 304 stainless steel with copper interlayer sheet 20(2010) 1829−1834

[24] J.J. del Coz Díaz, P. Menéndez Rodríguez, P.J. García Nieto, D. Castro-Fresno Comparative analysis of TIG welding distortions between austenitic and duplex stainless steels by FEM [2010] 30 (2010) 2448e2459

[25] D Liang, J W Soward, G S Frankel, B T Alexandrov, J C Lippold. Corrosion resistance of welds in type 304L stainless steel made with a nickel–copper–ruthenium welding consumable [J]. Corrosion Science, 2010, 52: 2439−2451.

[26] M. Weigl, M. Schmid Influence of the feed rate and the lateral beam displacement on the joining quality of laser-welded copper-stainless steel connections 5 (2010) 53‑59

[27] J.L. Song, S.B. Lin, C.L. Yang, G.C. Ma, H. Liu Spreading behavior and microstructure characteristics of dissimilar metals TIG welding–brazing of aluminum alloy to stainless steel [2009] 509 (2009) 31–40

[28] Nilesh Pohokar, Lalit Bhuyar Neural Networks Based Approach for Machining and Geometric Parameters optimization of a CNC End Milling. ISSN: 2319-8753, Vol. 3, Issue 2, February 2014

[29] Montgomery D.C, 2006, "Design and analysis of Experiments" Wiley-INDIA edition

[30] https://explorable.com/factorial-design

[31] S. Deivanai, Dr Reeta Wattal, Mrs Sudhali Rani, Ms Surabhi Lata Heat Flow prediction in fiction stir welded aluminium, International Journal of Mechanical Engineering and Technology, volume 5, Issue 9, September (2014) pp. 336-346.

[32] http://en.wikipedia.org/wiki?curid=1710040

[33] http://www.pakiemak.com/2006/03/quick-facts-on-stainless-steel.html

[34] http://www.scribd.com/doc/78837372/Diagram-Fasa

[35] http://amsresources.com/c10100-oxygen-free-electronic-copper-ofec-or-ofhc

[36] Experimental and theory study on the effect of welding speed and tool pin profile on aluminium friction stir welded butt joints Vijay Kumar T1, B.Sridhar Babu2, Rakesh Jalla3.

[37] R.S. Parmar, Welding Process and Technology, Second edition, Khanna Publication.